Published for SISSA by Springer

Received: July 6, 2023
Accepted: July 14, 2023
Published: July 28, 2023

The ABC of RPV: classification of R-parity violating signatures at the LHC for small couplings

Herbi K. Dreiner,[a] **Yong Sheng Koay,**[b] **Dominik Köhler,**[a] **Víctor Martín Lozano,**[c,d] **Javier Montejo Berlingen,**[e,f] **Saurabh Nangia**[a] **and Nadja Strobbe**[g]

[a] *Bethe Center for Theoretical Physics & Physikalisches Institut der Universität Bonn, Nußallee 12, 53115 Bonn, Germany*

[b] *Department of Physics and Astronomy, Uppsala University, Box 516, SE-751 20 Uppsala, Sweden*

[c] *Departament de Física Teòrica, Universitat de València-CSIC, E-46100, Burjassot, Spain*

[d] *Instituto de Física Corpuscular, CSIC-Universitat de València, 46980 Paterna, Spain*

[e] *Instituto de Física de Altas Energías, Campus UAB, 08193, Bellaterra (Barcelona), Spain*

[f] *International Center for Quantum-field Measurement Systems for Studies of the Universe and Particles (QUP), 1-1 Oho, Tsukuba, Ibaraki 305-0801, Japan*

[g] *School of Physics & Astronomy, University of Minnesota, Minneapolis, MN 55455, U.S.A.*

E-mail: dreiner@uni-bonn.de, yongsheng.koay@physics.uu.se, koehler@physik.uni-bonn.de, victor.lozano@ific.uv.es, jmontejo@cern.ch, nangia@physik.uni-bonn.de, nstrobbe@umn.edu

https://doi.org/10.1007/JHEP07(2023)215

JHEP07(2023)215

Abstract: We perform a classification of all potential supersymmetric R-parity violating signatures at the LHC to address the question: *are existing bounds on supersymmetric models robust, or are there still signatures not covered by existing searches, allowing LHC-scale supersymmetry to be hiding?* We analyze all possible scenarios with one dominant RPV trilinear coupling at a time, allowing for arbitrary LSPs and mass spectra. We consider direct production of the LSP, as well as production via gauge-cascades, and find 6 different experimental signatures for the $LL\bar{E}$-case, 6 for the $LQ\bar{D}$-case, and 5 for the $\bar{U}\bar{D}\bar{D}$-case; together these provide complete coverage of the RPV-MSSM landscape. This set of signatures is confronted with the existing searches by `ATLAS` and `CMS`. We find all signatures have been covered at the LHC, although not at the sensitivity level needed to probe the direct production of all LSP types. For the case of a dominant $LL\bar{E}$-operator, we use `CheckMATE` to quantify the current lower bounds on the supersymmetric masses and find the limits to be comparable to or better than the R-parity conserving case. Our treatment can be easily extended to scenarios with more than one non-zero RPV coupling.

Keywords: Supersymmetry, Specific BSM Phenomenology

ArXiv ePrint: 2306.07317

JHEP07(2023)215

Contents

JHEP07(2023)215

1 Introduction

Supersymmetry (SUSY) [1–4] is a well-motivated extension of the Standard Model (SM). It uniquely extends the SM algebra [5, 6], addresses the 'naturalness problem' of the Higgs boson [7, 8], and has many further appealing features, as reviewed in refs. [9–11]. Extensive experimental effort has been devoted in its search, particularly at the Large Hadron Collider (LHC) by the `ATLAS` and `CMS` Collaborations. However, no evidence for SUSY has been

found so far with lower mass bounds reaching $\mathcal{O}(1-2)$ TeV for the colored sector [12–35], and $\mathcal{O}(100-1000)$ GeV for the electroweak sector [12, 25, 27, 28, 36–51], with some dependence on the model details.

As we prepare for more data through Run 3 at the LHC, and especially in the high-luminosity era, it is an excellent opportunity to assess the current status of supersymmetric searches and gain insight into how we should proceed. An interesting question is: *Are the above bounds robust, or are there gaps/loopholes that could still allow LHC-scale SUSY to be hiding?* Typically, ATLAS and CMS derive these limits within the framework of various simplified models or a limited number of complete models such as the Constrained Minimal Supersymmetric Standard Model (CMSSM); it is not clear whether these results can be used to conclude that low-scale SUSY has been definitively excluded.

The above question was first addressed in ref. [52], and — after LHC Run 1 — in ref. [53], in more detail. In the latter, it was argued that any 'natural' SUSY model[1] with kinematically accessible gluinos — independent of model details — results in final states containing at least one of the following ingredients: large missing transverse momentum ($E_{\mathrm{T}}^{\mathrm{miss}}$), high multiplicity of objects (≥ 8), or a significant number of top quarks. Using this, the authors showed that combining just five existing ATLAS and CMS searches, and one newly proposed search [54] excludes almost any 'natural' SUSY model containing gluinos lighter than 1 TeV. Of course, using current data and a similar strategy should yield a higher mass bound. Nevertheless, the demonstration that a minimal set of searches can target almost any SUSY setup, independent of details concerning the model, mass spectrum, UV-completion, etc., is noteworthy. Such an approach is desirable, especially since it informs us about potential gaps that may exist in our SUSY coverage. For instance, the search proposed by ref. [54] represented a real gap that has since been filled by ATLAS and CMS in refs. [55, 56].

In this work, we wish to consider the same question but with two important differences. First, beyond assuming the MSSM particle content, we remain completely blind to the particle-spectrum details. In particular, we do not require that the gluinos are kinematically accessible. With the LHC transitioning from an era of energy upgrades to one of increasing luminosity, we should seriously entertain the possibility that the colored sector may be heavy, while a focus on rarer production channels may yield fruit. We also do not make any 'naturalness' requirements in the sense of ref. [53].

Second, our focus will be on the R-parity Violating MSSM (RPV-MSSM). The most general, renormalizable superpotential with the MSSM particle content includes lepton- and baryon-number violating operators, together referred to as RPV terms [10, 57–59]. These are usually set to zero by imposing a discrete $\mathbb{Z}_2$-symmetry called R-parity as they can lead to proton decay [60, 61] at rates in excess of the strict experimental bound [62]. However, the proton-decay problem can be averted without removing all RPV terms [63–65]; in general, there is no theoretical or phenomenological reason to consider the MSSM without RPV terms [58]. On the other hand, as we demonstrate in section 2, the different configurations of couplings and types of the lightest SUSY particle (LSP) in the

[1]The 'naturalness' criterion in ref. [53] requires the Higgsinos and stops to be light.

JHEP07(2023)215

RPV-MSSM lead to a bewildering number of possible signatures. In particular, with the requirements on gluino and higgsino masses absent, a large number of these signatures do not possess any of the characteristics listed in ref. [53]. In comparison, the 'vanilla' MSSM is less interesting as it tends to retain its characteristic significant E_T^{miss} signal, irrespective of spectrum details.[2] This makes a systematic treatment and classification particularly crucial in the case of the RPV-MSSM.

To summarize, we study the coverage of the most general RPV-MSSM setup at the LHC, without making any assumptions about the particle-spectrum details. We seek a minimal set of searches that would provide complete coverage; this will allow us to identify any potential gaps in our current searches. We will restrict ourselves to the case of small RPV couplings in this work, leaving the large-coupling case for a dedicated study in the future. Thus, the production of sparticles is unchanged from the MSSM case and we only need to consider pair-production channels. The final state signatures will be altered, however, due to the RPV couplings affecting decays.

The paper is organized as follows. In section 2, we set notation and state the assumptions of our framework. Further, we explicitly describe the vast phenomenology of the RPV-MSSM, in order to demonstrate our point about the need for a systematic method of classification. In section 3, we provide such a systematic classification by grouping signatures in a meaningful way, according to the coupling and nature of the LSP. Our approach allows us to identify a minimal set of searches that would provide complete RPV-MSSM coverage at the LHC, and discuss the current status of such a program. Then, in section 4, we demonstrate applications of our framework — as a first study — for the case of a dominant $LL\bar{E}$ RPV-operator. We consider several benchmark scenarios with such lepton-number violating operators, involving the full range of LSP types, and derive exclusion limits. Our results demonstrate that, irrespective of model details, the minimal set of searches proposed in this work can be used to derive strong limits. Finally, we conclude and discuss the implications and limitations of our work, and provide an outlook in section 5. Additionally, we provide a set of appendices containing supplementary details about our simulation procedure (section A), information that can be used to optimize future searches (section B), and an introduction to `abc-rpv` (section C), an accompanying RPV Python library[3] that can be used to generate all the signature tables in this paper.

2 Framework

2.1 Conventions and assumptions

With the MSSM particle content and the $N = 1$ supersymmetry algebra, the most general $\mathrm{SU}(3)_C \times \mathrm{SU}(2)_L \times \mathrm{U}(1)_Y$-invariant, renormalizable superpotential is,

$$W = W_{\text{MSSM}} + W_{\text{LNV}} + W_{\text{BNV}}\,, \tag{2.1}$$

[2] We note that the E_T^{miss} signature can be diluted even in the case of the MSSM through scenarios with a compressed spectrum or a 'Hidden Valley'; see, for instance, refs. [53, 66] for details. Despite the varied phenomenology offered by these models, we believe that it is more efficient to thoroughly explore the minimal setup provided by the RPV-MSSM before adding further complexities.

[3] Available at: https://github.com/kys-sheng/abc-rpv.git.

JHEP07(2023)215

where $W_{\rm MSSM}$ is the usual MSSM superpotential — see, for instance, ref. [67] — while,

$$W_{\rm LNV} = \frac{1}{2}\lambda^{ijk} L_i L_j \bar{E}_k + \lambda'^{ijk} L_i Q_j \bar{D}_k + \kappa^i H_u L_i \,, \qquad W_{\rm BNV} = \frac{1}{2}\lambda''^{ijk} \bar{U}_i \bar{D}_j \bar{D}_k \,, \tag{2.2}$$

violate lepton- and baryon-number, respectively. Together, $W_{\rm RPV} \equiv W_{\rm LNV} + W_{\rm BNV}$, are called the RPV superpotential terms. In our notation, L ($\bar{E}$) and Q ($\bar{U}$, $\bar{D}$) are the MSSM lepton- and quark-doublet (-singlet) chiral superfields, respectively, while H_u labels the (up-type) SU(2)$_L$-doublet Higgs chiral superfield. We do not write gauge indices explicitly but retain the generational ones: $i, j, k \in \{1, 2, 3\}$ with a summation implied over repeated indices. The λ's and the κ's are the trilinear and bilinear couplings, respectively.

We shall employ the particle content of the MSSM and the superpotential of eq. (2.1) as the basis for this study. As mentioned in the Introduction, some terms in the superpotential can lead to rapid proton decay. In general, this requires combinations of certain $LQ\bar{D}$ and $\bar{U}\bar{D}\bar{D}$ operators.[4] As long as these combinations are kept small, the proton's lifetime remains consistent with the bounds. Indeed, there are symmetries that can achieve this — see, for instance, refs. [63–65]. In this study, we will not bother with the details of how this is done; our focus will be on classifying all possible collider signatures coming from the various couplings. We will, however, ignore the bilinear couplings. These are severely constrained by neutrino mass data [67] and are expected to be relevant for colliders only in limited contexts [59, 68]. Furthermore, at a fixed energy scale they can be rotated away [69, 70].

The optimal search strategy for RPV-MSSM scenarios at colliders depends on the magnitude of the RPV couplings. We will restrict ourselves to the case where these couplings are small enough such that the production of sparticles and their cascade decays down to the LSP remain unchanged from the MSSM case, but large enough so that the LSP decays promptly in the detector (we also require the cascade decays of the other sparticles to be prompt). While the exact magnitudes depend on the spectrum details, we can estimate it to roughly mean the range,

$$\sqrt{\frac{(\beta\gamma)\, 10^{-12}\,\text{GeV}}{m_{\rm LSP}}} \lesssim \lambda \ll g \,, \tag{2.3}$$

where λ is the relevant RPV coupling, g is a gauge coupling, $m_{\rm LSP}$ is the mass of some LSP that has a two body-decay via the RPV coupling, and β and γ are its velocity and Lorentz factor, respectively. The left condition is derived from the requirement that the LSP has a decay length of about 1 cm in the lab frame.[5] For an LSP mass of 1 TeV, eq. (2.3) implies the range $\mathcal{O}\left(10^{-7}\right) \lesssim \lambda \ll \mathcal{O}\left(10^{-1}\right)$. Considering λ values smaller or larger than the above range leads to unique features that require separate studies. The former can lead to new kinds of signals such as displaced vertices or long-lived particles, and both topics have received some attention in recent times [71–82]. The latter also leads to interesting

[4] One exception is if the lightest neutralino is lighter than the proton in which case the decay can occur via $\bar{U}\bar{D}\bar{D}$ operators alone [61].

[5] We have considered a two-body decay here. For comparison, a similar estimate for an LSP with mass 500 GeV undergoing a three-body decay via a virtual sfermion of mass 1 TeV (this is how a neutralino decays, for instance) gives the range $\mathcal{O}\left(10^{-5}\right) \lesssim \lambda \ll \mathcal{O}\left(10^{-1}\right)$. We note that, in some cases, four-body decays are also possible, e.g., a slepton LSP decaying via λ'' couplings.

JHEP07(2023)215

Symbol	Particles
ℓ	e/μ
L	ℓ/τ
j_l	$u/d/c/s$ jets
j_3	t/b jets
j	j_l/j_3 jets
V	$W/Z/h$
$\tilde{\ell}(\tilde{\nu})$	$\tilde{e}_L(\tilde{\nu}_e)/\tilde{\mu}_L(\tilde{\nu}_\mu)$
$\tilde{e}$	$\tilde{e}_R/\tilde{\mu}_R$
$\tilde{q}$	$\tilde{u}_L/\tilde{d}_L/\tilde{c}_L/\tilde{s}_L$
$\tilde{u}$	$\tilde{u}_R/\tilde{c}_R$
$\tilde{d}$	$\tilde{d}_R/\tilde{s}_R$
$\tilde{q}_3$	$\tilde{t}_L/\tilde{b}_L$
$\tilde{t}$	$\tilde{t}_R$
$\tilde{b}$	$\tilde{b}_R$
$\tilde{B}$	Bino
$\tilde{W}$	Winos (charged/neutral)
$\tilde{H}$	Higgsinos (charged/neutral)

Table 1. Summary of notation for labeling the RPV-MSSM particle content used in this work. For the particles not mentioned in the table, we use standard notation.

features; in particular, single production of sparticles [83–87], and RPV effects in cascade chains can lead to phenomenological changes requiring a dedicated study that we shall pursue in the future, as a continuation of this work.

One assumption, related to the above point, that we will need to make in this work is that the LSP is not too light, i.e., $m_{\rm LSP} > \mathcal{O}\,(200\,{\rm GeV})$. While current mass bounds on most SUSY particles place them well above this limit, a bino-like neutralino is still allowed to be massless [88, 89]. Requiring the above condition ensures that the decay of the LSP can be prompt without requiring the RPV couplings to be too large. Further, it allows the LSP to decay into all SM fermions (except for, perhaps, the top quark).[6] Dedicated LHC studies for a very light neutralino can be found in, for instance, refs. [90–92].

Finally, before concluding this subsection, we introduce our notation for labeling the particle content in table 1. We will find the groupings we define useful in presenting our results later. For simplicity, we will also assume all SUSY particles belonging to a particular grouping are mass degenerate — i.e., we treat mass splittings between components of the same doublet (for instance, $\tilde{H}^\pm$ and $\tilde{H}^0$), as well as between first and second generation sparticles as negligible. The former assumption holds true to a very good approximation [10]. The latter is not essential for our framework but allows us to be concise; generalization is straightforward.

[6]Note that, throughout this work, we will neglect all SM Yukawas, except for that of the top quark.

JHEP07(2023)215

2.2 The RPV landscape

The presence of even small RPV couplings can drastically change collider phenomenology compared to the MSSM. In the latter case, SUSY particles are pair-produced at colliders and undergo gauge-cascade decays into the LSP — typically the neutralino[7] — which then escapes the detector unobserved, giving the characteristic E_T^{miss} signature. The presence of RPV couplings changes this simple picture in two main ways. First, the LSP is no longer constrained to be the neutralino but can be any SUSY particle [94, 95]. Second, the RPV couplings make the LSP unstable; the E_T^{miss} signature is now replaced (diluted, or even completely absent) by the objects arising in this decay, which are determined by the dominant RPV coupling. The total number of possible signatures for the RPV-MSSM at a hadron collider can be summarized as (adapted from ref. [95], see also ref. [96]):

$$\text{RPV signature} = \begin{pmatrix} \tilde{g}\tilde{g} \\ \tilde{g}\tilde{q}, \tilde{g}\tilde{u}\ldots \\ \tilde{q}\tilde{q}, \tilde{q}_3\tilde{q}_3, \tilde{q}\tilde{u}\ldots \\ \tilde{\ell}\tilde{\ell}, \tilde{\tau}_L\tilde{\tau}_L, \tilde{\ell}\tilde{\nu}\ldots \\ \tilde{H}\tilde{H} \\ \tilde{W}\tilde{W} \\ \tilde{B}\tilde{B} \end{pmatrix}_{\substack{\text{Production} \\ \text{Channels}}} \otimes \begin{pmatrix} \tilde{B} \\ \tilde{H} \\ \tilde{W} \\ \tilde{\ell}(\tilde{\nu}) \\ \tilde{\tau}_L(\tilde{\nu}_\tau) \\ \tilde{e} \\ \tilde{\tau}_R \\ \tilde{q} \\ \tilde{u} \\ \tilde{d} \\ \tilde{q}_3 \\ \tilde{t} \\ \tilde{b} \\ \tilde{g} \end{pmatrix}_{\substack{\text{Possible} \\ \text{LSPs}}} \otimes \begin{pmatrix} L_1L_2\bar{E}_1 \\ \ldots \\ L_1Q_1\bar{D}_1 \\ \ldots \\ \bar{U}_3\bar{D}_2\bar{D}_3 \end{pmatrix}_{\substack{\text{LSP} \\ \text{Decay}}} \tag{2.4}$$

There are 45 different RPV trilinear couplings to consider above. Further, the final state will depend on the details of the cascade decays which, in turn, are determined by the mass orderings in the SUSY spectrum: the total number of possibilities is immense! The first systematic analysis of these signatures was performed in ref. [84], for the particular case of a neutralino LSP. A more general classification, allowing for all possible LSPs, has been presented in ref. [96] (see also ref. [97]). However, the study assumes that the lightest colored particle is kinematically accessible at the collider. In this work, we extend this by also including the possibility that the colored sector lies beyond LHC energies. More importantly, the emphasis in ref. [96] was on finding signatures arising most frequently from eq. (2.4), when one considers the space of all possible mass orderings of the SUSY spectrum. Our approach here is different: we wish to create a minimal set of signatures that provides complete coverage for the space of RPV-MSSM models, irrespective of how frequently an individual signature may arise. Furthermore, we will concretely tie this to the LHC search

[7] The nature of the LSP in the MSSM follows from the strict constraints on charged or colored stable particles [59, 93].

JHEP07(2023)215

program, discussing the current experimental coverage and identifying possible gaps; this aspect is absent in ref. [96]. Ref. [95] has studied it for the case of the RPV-CMSSM, but a more general model-independent treatment is missing in the literature.

3 Classification of signatures: the RPV dictionary

We now describe our approach for classifying the most general RPV-MSSM signatures. Since we assume the RPV couplings are small, sparticles are pair-produced at the LHC via gauge interactions, as in the MSSM. The production channels that we consider are listed in eq. (2.4) on the left; the mass spectrum determines which of these are kinematically accessible. The produced sparticles — if not the LSP — will then cascade-decay via gauge interactions until the LSP is reached with the details of the cascade also depending on the model (i.e., the spectrum). The LSP, once produced, decays promptly via the relevant RPV coupling.

In our model-independent approach, we target the last step above: the LSP decay. The essential features of the signatures can be characterized by specifying the nature of the LSP and the RPV coupling, independent of any spectrum-specific details such as the exact chain leading to the LSP production, the mass hierarchies, etc. This is obviously true when the LSP couples directly to the relevant RPV decay operator, leading to a two-body decay. However, it is also true more generally. To illustrate this point, we consider a scenario with a $\tilde{q}$ LSP (first or second generation squark doublet, cf. table 1), with λ''_{312} the only non-zero RPV coupling. In this case, there is no direct two-body decay available for $\tilde{q}$. Instead, it must decay via a virtual $\tilde{t}$ or $\tilde{d}$; some of the paths it can take are depicted in figure 1. Without specifying the model spectrum, it is impossible to state which path will be favored. However, note that in each case we end up with the final state $t + 3j_l + X$.[8] This is a general feature, independent of the path it actually takes. Thus, any model with a $\tilde{q}$ LSP and a dominant λ''_{312} operator has a characteristic $t + 3j_l$ signature, irrespective of any other spectrum details. We can target all such scenarios with a single search — this observation is the most crucial aspect of this work.

Using the above approach, we can compile the characteristic signatures arising from each LSP and dominant RPV coupling combination, in order to arrive at a minimal set of searches that would provide complete coverage for the RPV-MSSM, in a model-independent way. We present this set in the form of tables below. We will also compare it to what has been covered by the vast program of BSM searches by the ATLAS and CMS collaborations. Although only a small subset of these searches provides an explicit interpretation in terms of RPV-SUSY models, the wide range of final states considered covers the majority of signatures expected from RPV decays. Thus, appropriately reinterpreted, they could be used to restrict the RPV parameter space.

In order to facilitate a systematic exploration of the RPV-MSSM landscape with our approach, we have developed an RPV Python library called `abc-rpv`. This library provides

[8] There is one subtlety here: the $\tilde{H}$ path in figure 1 leads to a b-jet instead of t if it proceeds via $\tilde{H}^{\pm}$. However, since we assume $\tilde{H}^{\pm}$ and $\tilde{H}^0$ are mass-degenerate, the corresponding path via $\tilde{H}^0$ is always equally likely.

JHEP07(2023)215

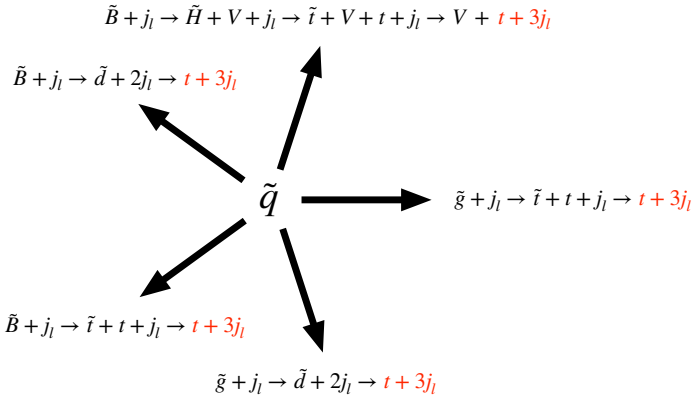

Figure 1. Some possible paths a $\tilde{q}$ LSP can take while decaying through λ''_{312}. Since $\tilde{q}$ is the LSP here, all the intermediate sparticles are virtual. See table 1 for the notation employed.

a powerful toolkit containing a range of features for analyzing the characteristic signatures arising from various RPV scenarios. The main functionalities include identifying signatures and decay chains for any LSP and RPV coupling combination, as well as going in the other direction: identifying potential RPV scenarios leading to a user-given final state. Using this library, one can reproduce all signature tables in this paper — for instance, (tables 2–11) shown below, as well as table 17 in section B. The information in figure 1 (possible decay chains for a given LSP) can also be generated easily up to a fixed number of vertices. An introduction to the `abc-rpv` library, including a quick user manual is provided in section C.

We note that one downside of our approach is that only final state objects arising in the LSP decay are targeted, and all objects arising in the cascade decays are neglected. In specific models — for instance, one with squark pair-production and a neutralino LSP — one could certainly optimize by targeting the additional jets arising in the cascade decays of the parent squarks, thus improving the search sensitivity. However, in order to analyze the status of complete coverage while being model-independent, our approach is necessary. For completeness, we compile a list of additional objects that can arise in cascade decays for various production channels in table 17 in section B. That table may be used to optimize the searches compiled below for particular scenarios when the model details are known. Further, it can help understand the loss in sensitivity for searches that veto additional objects to help with background suppression.

3.1 LLE tables

We depict the signatures corresponding to the decay of a pair of LSPs for the $LL\bar{E}$ operators of eq. (2.2) in tables 2 and 3. The tables have been written assuming that LSPs are gauge eigenstates, and the pair decays via the same coupling. However, if one is interested in scenarios where the mass eigenstates have significant mixing, or where several dominant RPV couplings contribute, the results can be generalized by considering linear combinations of the table entries.

The tables show the LSP in the first column. The second and third columns depict the resulting signature depending on the generation structure of the $LL\bar{E}$ operator responsible

JHEP07(2023)215

LSP	LLE	$\mathbf{LL_3E}$
$\tilde{\ell}\,(\tilde{\nu})$	$3\ell + E_T^{\rm miss}/4\ell$	$2\ell + \tau + E_T^{\rm miss}/2\ell + 2\tau$
$\tilde{e}$	$2\ell + E_T^{\rm miss}$	$2\ell + E_T^{\rm miss}/\ell + \tau + E_T^{\rm miss}$
$\tilde{\tau}_L\,(\tilde{\nu}_\tau)$	$4\ell + 2\tau + E_T^{\rm miss}/4\ell + \tau + E_T^{\rm miss}$	$3\ell + E_T^{\rm miss}/4\ell$
$\tilde{\tau}_R$	$4\ell + 2\tau + E_T^{\rm miss}$	$4\ell + 2\tau + E_T^{\rm miss}/3\ell + 3\tau + E_T^{\rm miss}$
$\tilde{g}$	$4\ell + 4j + E_T^{\rm miss}$	$4\ell + 4j + E_T^{\rm miss}/3\ell + \tau + 4j + E_T^{\rm miss}$
$\tilde{q},\ \tilde{u},\ \tilde{d}$	$4\ell + 2j_l + E_T^{\rm miss}$	$4\ell + 2j_l + E_T^{\rm miss}/3\ell + \tau + 2j_l + E_T^{\rm miss}$
$\tilde{t}_L(\tilde{b}_L)$	$4\ell + 2j_3 + E_T^{\rm miss}$	$4\ell + 2j_3 + E_T^{\rm miss}/3\ell + \tau + 2j_3 + E_T^{\rm miss}$
$\tilde{t}_R$	$4\ell + 2t + E_T^{\rm miss}$	$4\ell + 2t + E_T^{\rm miss}/3\ell + \tau + 2t + E_T^{\rm miss}$
$\tilde{b}_R$	$4\ell + 2b + E_T^{\rm miss}$	$4\ell + 2b + E_T^{\rm miss}/3\ell + \tau + 2b + E_T^{\rm miss}$
$\tilde{B},\ \tilde{W},\ \tilde{H}$	$4\ell + E_T^{\rm miss}$	$4\ell + E_T^{\rm miss}/3\ell + \tau + E_T^{\rm miss}$

Table 2. Characteristic signatures arising from LSP decays for $L_iL_j\bar{E}_k$ operators. The first column depicts the LSPs. The second and third columns represent the signatures from *pair-production* of LSPs for the cases where the indices $i, j, k \in \{1, 2\}$, and where the indices $i, k \in \{1, 2\}$ and $j = 3$, respectively. For cases involving degenerate LSPs, e.g., $\tilde{\ell}\,(\tilde{\nu})$, all pair combinations are considered. Further, only the relevant signatures are retained and we have introduced color-coding to improve the readability of the table; the details are in the main text.

LSP	$\mathbf{LLE_3}$	$\mathbf{LL_3E_3}$
$\tilde{\ell}\,(\tilde{\nu})$	$\ell + 2\tau + E_T^{\rm miss}/2\ell + 2\tau$	$3\tau + E_T^{\rm miss}/4\tau$
$\tilde{e}$	$4\ell + 2\tau + E_T^{\rm miss}$	$4\ell + 2\tau + E_T^{\rm miss}/3\ell + 3\tau + E_T^{\rm miss}$
$\tilde{\tau}_L\,(\tilde{\nu}_\tau)$	$2\ell + 4\tau + E_T^{\rm miss}/2\ell + 3\tau + E_T^{\rm miss}$	$2\ell + 2\tau/\ell + 2\tau + E_T^{\rm miss}$
$\tilde{\tau}_R$	$2\ell + E_T^{\rm miss}$	$2\ell + E_T^{\rm miss}/\ell + \tau + E_T^{\rm miss}$
$\tilde{g}$	$2\ell + 2\tau + 4j + E_T^{\rm miss}$	$2\ell + 2\tau + 4j + E_T^{\rm miss}/\ell + 3\tau + 4j + E_T^{\rm miss}$
$\tilde{q},\ \tilde{u},\ \tilde{d}$	$2\ell + 2\tau + 2j_l + E_T^{\rm miss}$	$2\ell + 2\tau + 2j_l + E_T^{\rm miss}/\ell + 3\tau + 2j_l + E_T^{\rm miss}$
$\tilde{t}_L(\tilde{b}_L),$	$2\ell + 2\tau + 2j_3 + E_T^{\rm miss}$	$2\ell + 2\tau + 2j_3 + E_T^{\rm miss}/\ell + 3\tau + 2j_3 + E_T^{\rm miss}$
$\tilde{t}_R$	$2\ell + 2\tau + 2t + E_T^{\rm miss}$	$2\ell + 2\tau + 2t + E_T^{\rm miss}/\ell + 3\tau + 2t + E_T^{\rm miss}$
$\tilde{b}_R$	$2\ell + 2\tau + 2b + E_T^{\rm miss}$	$2\ell + 2\tau + 2b + E_T^{\rm miss}/\ell + 3\tau + 2b + E_T^{\rm miss}$
$\tilde{B},\ \tilde{W},\ \tilde{H}$	$2\ell + 2\tau + E_T^{\rm miss}$	$2\ell + 2\tau + E_T^{\rm miss}/\ell + 3\tau + E_T^{\rm miss}$

Table 3. Same as table 2 but for $L_iL_j\bar{E}_k$ operators with $i, j \in \{1, 2\}$ and $k = 3$ (second column), and $j, k = 3$ and $i \in \{1, 2\}$ (third column).

JHEP07(2023)215

for decay; we employ the compact notation of table 1. Note that, to be concise, we assume all RPV operators within a given category are non-zero, e.g., both $L_1L_2\bar{E}_1$ and $L_1L_2\bar{E}_2$ are non-zero for the category $LL\bar{E}$. Otherwise, more objects may arise, e.g., with a $\tilde{\mu}_R$ LSP and a non-zero $L_1L_2\bar{E}_1$ operator, the smuon would first need to transition into $\tilde{\ell}(\tilde{\nu})$ or $\tilde{e}_R$ leading to two extra muons; the extension is straightforward. In some cases, there is more than one signature possible. If two signatures are equally likely, we have listed the one that contains more electrons or muons, since we expect it to be more readily observable. In cases where a signature with fewer e/μ can have a higher cross-section, we have retained both separated by a '/'. For instance, in the case of a $\tilde{\ell}(\tilde{\nu})$ LSP (we assume mass degeneracy of $\mathrm{SU}(2)_L$-doublets, cf. table 1) decaying via λ_{121}, the $\tilde{\ell}$ decays into one charged lepton and one neutrino, while the $\tilde{\nu}$ decays into two charged leptons. Thus, the possible signatures from pair production are: 4ℓ, $3\ell + E_T^{\mathrm{miss}}$, $2\ell + E_T^{\mathrm{miss}}$. In the table, we retain the first and second signatures: the former because it has the highest number of charged leptons, and the latter because it has the highest cross-section. $2\ell + E_T^{\mathrm{miss}}$ is not retained since it has both a lower cross-section compared to the $3\ell + E_T^{\mathrm{miss}}$ signature, as well as fewer leptons and, hence, will never be the most relevant final state for searches.

From the tables, we see that the $LL\bar{E}$ case can be completely covered through the following six searches:

1. $2L + E_T^{\mathrm{miss}}$
2. $3L + E_T^{\mathrm{miss}}$
3. $4L$
4. $4L + (0-4)j + E_T^{\mathrm{miss}}$
5. $5L + E_T^{\mathrm{miss}}$
6. $6L + E_T^{\mathrm{miss}}$

To improve the readability of the table, we have introduced a color scheme based on the number of charged leptons in the search region: red (two), blue (three), yellow (four without missing energy), green (four with missing energy), purple (five), and gray (six).

Thus, indeed — in spite of the large number of possibilities that RPV offers — it is possible to organize experimental searches into a small, workable set. The identification of these minimal signatures and the corresponding experimental coverage is one of the main results of this paper. We stress that this is more than just a convenient notational scheme. As will be shown, all signatures that we will classify in our tables — except for one — are experimentally covered by ATLAS and CMS in one form or another, although in some cases strong improvements in sensitivity are required to reach the electroweak production cross-sections. In section 4, we will further apply these to see how the same small set of searches provides exclusion limits across a broad class of RPV models.

One point to note is that, in the above, we have only classified the total number of leptons in each search. However, often it may be useful to know the flavor/sign combinations of these leptons. While we do not employ them in our numerical studies, we provide tables

JHEP07(2023)215

in section B that explicitly show these configurations. These may be useful in developing more sensitive search regions, in case one wishes to target specific scenarios.

We now discuss the experimental coverage of the above signatures. The six final states identified include multiple leptons, may include additional jets, and may come with or without E_T^{miss}. Searches for R-parity Conserving SUSY (RPC-SUSY) typically have good coverage for signatures with E_T^{miss} or with at least three leptons (or two with the same charge), with several of these searches providing some interpretations in RPV-SUSY models as well. Other searches sensitive to the $LL\bar{E}$ case include analyses targeting heavy leptons or additional Higgs bosons. LHC searches relevant for the $LL\bar{E}$ coupling broadly span the final states of (1.) $2\ell + E_T^{\text{miss}}$ [27–29, 41, 46, 47, 51, 98, 99], (2.) $3\ell + E_T^{\text{miss}}$ [27, 29, 38, 43, 100, 101], (3.) 4ℓ [43, 102–106], and (4., 5., 6.) $\geq 4\ell + E_T^{\text{miss}}$ [29, 43, 101, 107]. Searches with four leptons are typically inclusive and include events with more than four leptons, therefore covering also the $5L$ and $6L$ categories.

3.2 UDD tables

Next, we show analogous results for the $\bar{U}\bar{D}\bar{D}$ case in tables 4 and 5. The comments from before apply here too. These scenarios can be completely covered through the following five searches:

1. $4j$
2. $2j_l + 4j$
3. $2j_l + 6j$
4. $1L + 2j_l + 4j + E_T^{\text{miss}}$
5. $2L + 2j_l + 4j$

The color scheme is based on the number of jets and charged leptons: red (four jets), blue (six jets, no leptons), yellow (eight jets), green (six jets, one lepton), and purple (six jets, two leptons).

One interesting point worth noting is that we write j_3 and not t in table 5 for the non-colored LSPs (j_3 indicates that the jet could be t/b, cf. table 1). This is to account for the possibility that kinematic suppression may lead to the decay into a b (via a virtual chargino) to be preferred over the decay into a t (via a neutralino). Generally, in all tables to follow, we will take this consideration into account for all the non-colored LSPs.

Three of the five $U\bar{D}\bar{D}$ final states listed above contain only jets and correspond to the largest fraction of the possible LSP decays. However, up to two of the jets listed could be top quarks in certain configurations. This would result in additional final state jets or leptons which can be used as experimental handles to improve sensitivity. The last two signatures listed arise from slepton LSPs and always include leptons and/or E_T^{miss} in the final state. ATLAS and CMS have covered the signatures of (1.) 4 jets [108–110], (2.) 6 jets [111, 112], (3.) 8 jets [56, 106, 113–115], (4.) 1 lepton plus at least 6 jets [31, 55, 56, 116, 117], and (5.) 2 leptons plus 6 jets [29, 117, 118].

JHEP07(2023)215

LSP	UDD	UD_3D
$\tilde{\ell}\,(\tilde{\nu})$	$2\ell + 6j_l/\ell + 6j_l + E_T^{\rm miss}$	$2\ell + 2b + 4j_l/\ell + 2b + 4j_l + E_T^{\rm miss}$
$\tilde{e}$	$2\ell + 6j_l$	$2\ell + 2b + 4j_l$
$\tilde{\tau}_L\,(\tilde{\nu}_\tau)$	$2\tau + 6j_l/\tau + 6j_l + E_T^{\rm miss}$	$2\tau + 2b + 4j_l/\tau + 2b + 4j_l + E_T^{\rm miss}$
$\tilde{\tau}_R$	$2\tau + 6j_l$	$2\tau + 2b + 4j_l$
$\tilde{g}$	$6j_l$	$2b + 4j_l$
$\tilde{q}$	$8j_l$	$2b + 6j_l$
$\tilde{u}$	$4j_l$	$2b + 2j_l$
$\tilde{d}$	$4j_l$	$2b + 2j_l$
$\tilde{t}_L(\tilde{b}_L)$	$6j_l + 2j_3$	$2b + 4j_l + 2j_3$
$\tilde{t}_R$	$2t + 6j_l$	$2t + 2b + 4j_l$
$\tilde{b}_R$	$2b + 6j_l$	$4j_l$
$\tilde{B},\ \tilde{W},\ \tilde{H}$	$6j_l$	$2b + 4j_l$

Table 4. Characteristic signatures arising from LSP decays for $\bar{U}_i\bar{D}_j\bar{D}_k$ operators. The first column depicts the LSPs. The second and third columns represent the signatures from *pair-production* of LSPs for the cases where the indices $i, j, k \in \{1, 2\}$, and where the indices $i, k \in \{1, 2\}$ and $j = 3$, respectively. For cases involving degenerate LSPs, e.g., $\tilde{\ell}\,(\tilde{\nu})$, all pair combinations are considered. Further, only the relevant signatures are retained and we have introduced color-coding to improve the readability of the table; the details are in the main text.

Some of these searches explicitly require a minimum number of b-tagged jets, whereas others are more inclusive. The searches considering leptons typically only consider electrons or muons, which reduces the sensitivity to scenarios featuring tau leptons. The searches for signatures (1.), (2.), and (3.) reduce the potentially overwhelming multijet background by requiring the presence of two same-mass resonances in each event. Even so, while some final states are nominally covered, the large difference in production cross-sections leads to exclusion limits being available for some production modes (e.g., $\tilde{g} \to 3j_l$) but still requiring orders of magnitude of improvement to reach others (e.g., $\tilde{H} \to 3j_l$).

3.3 LQD tables

Lastly, we show the results for the $LQ\bar{D}$ case in tables 6–11. The comments from before apply here. Analyzing the tables, we see that the $LQ\bar{D}$ scenarios can be completely covered through the following six searches:

1. $4j$
2. $2b + 2j + E_T^{\rm miss}$

JHEP07(2023)215

LSP	U_3DD	U_3D_3D
$\tilde{\ell}\,(\tilde{\nu})$	$2\ell + 4j_l + 2j_3/\ell + 4j_l + 2j_3 + E_T^{\text{miss}}$	$2\ell + 2b + 2j_l + 2j_3/\ell + 2b + 2j_l + 2j_3 + E_T^{\text{miss}}$
$\tilde{e}$	$2\ell + 4j_l + 2j_3$	$2\ell + 2b + 2j_l + 2j_3$
$\tilde{\tau}_L\,(\tilde{\nu}_\tau)$	$2\tau + 4j_l + 2j_3/\tau + 4j_l + 2j_3 + E_T^{\text{miss}}$	$2\tau + 2b + 2j_l + 2j_3/\tau + 2b + 2j_l + 2j_3 + E_T^{\text{miss}}$
$\tilde{\tau}_R$	$2\tau + 4j_l + 2j_3$	$2\tau + 2b + 2j_l + 2j_3$
$\tilde{g}$	$2t + 4j_l$	$2t + 2b + 2j_l$
$\tilde{q}$	$2t + 6j_l$	$2t + 2b + 4j_l$
$\tilde{u}$	$2t + 6j_l$	$2t + 2b + 4j_l$
$\tilde{d}$	$2t + 2j_l$	$2t + 2b$
$\tilde{t}_L(\tilde{b}_L)$	$4j_l + 4j_3$	$2b + 2j_l + 4j_3$
$\tilde{t}_R$	$4j_l$	$2b + 2j_l$
$\tilde{b}_R$	$2t + 2b + 4j_l$	$2t + 2j_l$
$\tilde{B},\ \tilde{W},\ \tilde{H}$	$4j_l + 2j_3$	$2b + 2j_l + 2j_3$

Table 5. Same as table 4 but for $\bar{U}_i\bar{D}_j\bar{D}_k$ operators with $j,k \in \{1,2\}$ and $i = 3$ (second column), and $i,j = 3$ and $k \in \{1,2\}$ (third column).

3. $1L + (2-6)j + E_T^{\text{miss}}$
4. $2L + (2-6)j + (E_T^{\text{miss}})$
5. $3L + 4j + E_T^{\text{miss}}$
6. $4L + 4j$

The color scheme is based on the number of charged leptons and jets: red (no charged leptons, four jets, without missing energy), blue (no charged leptons, four jets, with missing energy), yellow (one charged lepton), green (two charged leptons), purple (three charged leptons), and gray (four charged leptons).

As can be seen from the tables, $LQ\bar{D}$ operators result in a wide range of possible final states, typically including at least one lepton and several jets. Therefore, searches targeting a wide range of BSM models beyond RPV-SUSY can be sensitive, e.g., searches for RPC-SUSY, leptoquarks, etc. It is important to consider whether one of the generation indices of the $L_iQ_j\bar{D}_k$ operator is 3 since this changes the experimental signature significantly. For example, searches explicitly requiring b-tagged jets typically are the most sensitive for $j,k = 3$. An operator with $i = 3$ requires searches exploiting final states with τ leptons. The relevant existing searches for the $LQ\bar{D}$ coupling cover the final states of (1.) 4 jets [108–110], (2.) ≥ 4 jets (including b-tags) plus E_T^{miss} [33, 34], (3.) 1ℓ plus 2 jets [119, 120] or 1ℓ plus 6 jets [26, 35, 55, 56, 116, 117], (4.) 2ℓ-same-sign plus 2 jets [121], or 2ℓ-same-sign plus 6 jets [23, 29], or 2ℓ-opposite-sign plus 2 or more jets [17, 22, 28, 32, 117, 122–125], (5.) 3ℓ plus 4 jets [29, 43, 126], and (6.) 4ℓ plus 4 jets [43, 107].

It is important to note that for signatures 1. ($4j$) and 2. ($2b + 2j + E_T^{\text{miss}}$), the relevant searches target strong production cross-sections. As seen from tables 7 to 11, these

JHEP07(2023)215

LSP	LQD	$\mathbf{LQD_3}$
$\tilde{\ell}\,(\tilde{\nu})$	$4j_l$	$2b+2j_l$
$\tilde{e}$	$4\ell+4j_l/3\ell+4j_l+E_T^{\rm miss}$	$4\ell+2b+2j_l/3\ell+2b+2j_l+E_T^{\rm miss}$
$\tilde{\tau}_L\,(\tilde{\nu}_\tau)$	$2\ell+2\tau+4j_l/\ell+2\tau+4j_l+E_T^{\rm miss}/$ $2\ell+\tau+4j_l+E_T^{\rm miss}/\ell+\tau+4j_l+E_T^{\rm miss}$	$2\ell+2\tau+2b+2j_l/\ell+2\tau+2b+2j_l+E_T^{\rm miss}/$ $2\ell+\tau+2b+2j_l+E_T^{\rm miss}/\ell+\tau+2b+2j_l+E_T^{\rm miss}$
$\tilde{\tau}_R$	$2\ell+2\tau+4j_l/\ell+2\tau+4j_l+E_T^{\rm miss}$	$2\ell+2\tau+2b+2j_l/\ell+2\tau+2b+2j_l+E_T^{\rm miss}$
$\tilde{g}$	$2\ell+4j_l/\ell+4j_l+E_T^{\rm miss}$	$2\ell+2b+2j_l/\ell+2b+2j_l+E_T^{\rm miss}$
$\tilde{q}$	$2\ell+2j_l$	$2\ell+2b$
$\tilde{u}$	$2\ell+6j_l/\ell+6j_l+E_T^{\rm miss}$	$2\ell+2b+4j_l/\ell+2b+4j_l+E_T^{\rm miss}$
$\tilde{d}$	$2\ell+2j_l/\ell+2j_l+E_T^{\rm miss}$	$2\ell+2b+4j_l/\ell+2b+4j_l+E_T^{\rm miss}$
$\tilde{t}_L(\tilde{b}_L)$	$2\ell+4j_l+2j_3/\ell+4j_l+2j_3+E_T^{\rm miss}$	$2\ell+2b+2j_l+2j_3/\ell+2b+2j_l+2j_3+E_T^{\rm miss}$
$\tilde{t}_R$	$2\ell+2t+4j_l/\ell+2t+4j_l+E_T^{\rm miss}$	$2\ell+2t+2b+2j_l/\ell+2t+2b+2j_l+E_T^{\rm miss}$
$\tilde{b}_R$	$2\ell+2b+4j_l/\ell+2b+4j_l+E_T^{\rm miss}$	$2\ell+2j_l/\ell+2j_l+E_T^{\rm miss}$
$\tilde{B},\ \tilde{W},\ \tilde{H}$	$2\ell+4j_l/\ell+4j_l+E_T^{\rm miss}$	$2\ell+2b+2j_l/\ell+2b+2j_l+E_T^{\rm miss}$

Table 6. Characteristic signatures arising from LSP decays for $L_iQ_j\bar{D}_k$ operators. The first column depicts the LSPs. The second and third columns represent the signatures from *pair-production* of LSPs for the cases where the indices $i,j,k\in\{1,2\}$, and where the indices $i,j\in\{1,2\}$ and $k=3$, respectively. For cases involving degenerate LSPs, e.g., $\tilde{\ell}\,(\tilde{\nu})$, all pair combinations are considered. Further, only the relevant signatures are retained and we have introduced color-coding to improve the readability of the table; the details are in the main text.

signatures arise from the decays $\tilde{\ell}\to jj$ and $\tilde{\chi}_1^0\to\nu jb$ respectively. While the latter is experimentally less sensitive than the competing $\tilde{\chi}_1^0\to\ell jt$ decay, phase-space effects due to the top-quark mass can lead to a strong suppression of channels involving t. In both cases, the existing analyses target strong production, via $\tilde{q}\to jj$ and $\tilde{g}\to bj\tilde{\chi}_1^0$, respectively,[9] and have no sensitivity to low masses and electroweak cross sections. We do note the special case of $\tilde{\chi}_1^0\to\nu bb$, leading to the $4b$+$E_T^{\rm miss}$ final state which has already been explored for Higgsino production [127, 128]. However, crucially, the searches require an intermediate Higgs resonance which is not present in the RPV case.

[9]The scenario with an almost massless neutralino matches the $LQ\bar{D}$ signature of $\tilde{g}\to bj\nu$.

JHEP07(2023)215

LSP	LQ_3D
$\tilde{\ell}\,(\tilde{\nu})$	$2j_l + 2j_3$
$\tilde{e}$	$4\ell + 2t + 2j_l / 3\ell + t + b + 2j_l + E_T^{\text{miss}} / 2\ell + 2b + 2j_l + E_T^{\text{miss}}$
$\tilde{\tau}_L\,(\tilde{\nu}_\tau)$	$2\ell + 2\tau + 2t + 2j_l / \ell + 2\tau + t + b + 2j_l + E_T^{\text{miss}} / 2\tau + 2b + 2j_l + E_T^{\text{miss}} / 2\ell + \tau + 2t + 2j_l + E_T^{\text{miss}} / \ell + \tau + t + b + 2j_l + E_T^{\text{miss}} / \tau + 2b + 2j_l + E_T^{\text{miss}}$
$\tilde{\tau}_R$	$2\ell + 2\tau + 2t + 2j_l / \ell + 2\tau + t + b + 2j_l + E_T^{\text{miss}} / 2\tau + 2b + 2j_l + E_T^{\text{miss}}$
$\tilde{g}$	$2\ell + 2t + 2j_l / \ell + t + b + 2j_l + E_T^{\text{miss}}$
$\tilde{q}$	$2\ell + 2t + 4j_l / \ell + t + b + 4j_l + E_T^{\text{miss}}$
$\tilde{u}$	$2\ell + 2t + 4j_l / \ell + t + b + 4j_l + E_T^{\text{miss}}$
$\tilde{d}$	$2\ell + 2t / \ell + t + b + E_T^{\text{miss}}$
$\tilde{t}_L(\tilde{b}_L)$	$2\ell + 2j_l$
$\tilde{t}_R$	$2\ell + 4t + 2j_l / \ell + 3t + b + 2j_l + E_T^{\text{miss}}$
$\tilde{b}_R$	$2\ell + 2t + 2b + 2j_l / \ell + t + 3b + 2j_l + E_T^{\text{miss}}$
$\tilde{B},\ \tilde{W},\ \tilde{H}$	$2\ell + 2j_l + 2j_3 / \ell + 2j_l + 2j_3 + E_T^{\text{miss}} / 2b + 2j_l + E_T^{\text{miss}}$

Table 7. Same as table 6 but for $L_iQ_j\bar{D}_k$ operators with $i,k \in \{1,2\}$ and $j = 3$.

LSP	LQ_3D_3
$\tilde{\ell}\,(\tilde{\nu})$	$2b + 2j_3$
$\tilde{e}$	$4\ell + 2t + 2b / 3\ell + t + 3b + E_T^{\text{miss}} / 2\ell + 4b + E_T^{\text{miss}}$
$\tilde{\tau}_L\,(\tilde{\nu}_\tau)$	$2\ell + 2\tau + 2t + 2b / \ell + 2\tau + t + 3b + E_T^{\text{miss}} / 2\tau + 4b + E_T^{\text{miss}} / 2\ell + \tau + 2t + 2b + E_T^{\text{miss}} / \ell + \tau + t + 3b + E_T^{\text{miss}} / \tau + 4b + E_T^{\text{miss}}$
$\tilde{\tau}_R$	$2\ell + 2\tau + 2t + 2b / \ell + 2\tau + t + 3b + E_T^{\text{miss}} / 2\tau + 4b + E_T^{\text{miss}}$
$\tilde{g}$	$2\ell + 2t + 2b / \ell + t + 3b + E_T^{\text{miss}}$
$\tilde{q}$	$2\ell + 2t + 2b + 2j_l / \ell + t + 3b + 2j_l + E_T^{\text{miss}}$
$\tilde{u}$	$2\ell + 2t + 2b + 2j_l / \ell + t + 3b + 2j_l + E_T^{\text{miss}}$
$\tilde{d}$	$2\ell + 2t + 2b + 2j_l / \ell + t + 3b + 2j_l + E_T^{\text{miss}}$
$\tilde{t}_L(\tilde{b}_L)$	$2\ell + 2b$
$\tilde{t}_R$	$2\ell + 4t + 2b / \ell + 3t + 3b + E_T^{\text{miss}}$
$\tilde{b}_R$	$2\ell + 2t / \ell + t + b + E_T^{\text{miss}}$
$\tilde{B},\ \tilde{W},\ \tilde{H}$	$2\ell + 2b + 2j_3 / \ell + 2b + 2j_3 + E_T^{\text{miss}} / 4b + E_T^{\text{miss}}$

Table 8. Same as table 6 but for $L_iQ_j\bar{D}_k$ operators with $j,k = 3$ and $i \in \{1,2\}$.

JHEP07(2023)215

LSP	$\mathbf{L_3QD}$	$\mathbf{L_3QD_3}$
$\tilde{\ell}\,(\tilde{\nu})$	$2\ell+2\tau+4j_l/2\ell+\tau+4j_l+E_T^{\rm miss}/$ $\ell+2\tau+4j_l+E_T^{\rm miss}/\ell+\tau+4j_l+E_T^{\rm miss}$	$2\ell+2\tau+2b+2j_l/2\ell+\tau+2b+2j_l+E_T^{\rm miss}/$ $\ell+2\tau+2b+2j_l+E_T^{\rm miss}/\ell+\tau+2b+2j_l+E_T^{\rm miss}$
$\tilde{e}$	$2\ell+2\tau+4j_l/2\ell+\tau+4j_l+E_T^{\rm miss}$	$2\ell+2\tau+2b+2j_l/2\ell+\tau+2b+2j_l+E_T^{\rm miss}$
$\tilde{\tau}_L\,(\tilde{\nu}_\tau)$	$4j_l$	$2b+2j_l$
$\tilde{\tau}_R$	$4\tau+4j_l/3\tau+4j_l+E_T^{\rm miss}$	$4\tau+2b+2j_l/3\tau+2b+2j_l+E_T^{\rm miss}$
$\tilde{g}$	$2\tau+4j_l/\tau+4j_l+E_T^{\rm miss}$	$2\tau+2b+2j_l/\tau+2b+2j_l+E_T^{\rm miss}$
$\tilde{q}$	$2\tau+2j_l$	$2\tau+2b$
$\tilde{u}$	$2\tau+6j_l/\tau+6j_l+E_T^{\rm miss}$	$2\tau+2b+4j_l/\tau+2b+4j_l+E_T^{\rm miss}$
$\tilde{d}$	$2\tau+2j_l/\tau+2j_l+E_T^{\rm miss}$	$2\tau+2b+4j_l/\tau+2b+4j_l+E_T^{\rm miss}$
$\tilde{t}_L(\tilde{b}_L)$	$2\tau+4j_l+2j_3/\tau+4j_l+2j_3+E_T^{\rm miss}$	$2\tau+2b+2j_l+2j_3/\tau+2b+2j_l+2j_3+E_T^{\rm miss}$
$\tilde{t}_R$	$2\tau+2t+4j_l/\tau+2t+4j_l+E_T^{\rm miss}$	$2\tau+2t+2b+2j_l/\tau+2t+2b+2j_l+E_T^{\rm miss}$
$\tilde{b}_R$	$2\tau+2b+4j_l/\tau+2b+4j_l+E_T^{\rm miss}$	$2\tau+2j_l/\tau+2j_l+E_T^{\rm miss}$
$\tilde{B},\ \tilde{W},\ \tilde{H}$	$2\tau+4j_l/\tau+4j_l+E_T^{\rm miss}$	$2\tau+2b+2j_l/\tau+2b+2j_l+E_T^{\rm miss}$

Table 9. Same as table 6 but for $L_iQ_j\bar{D}_k$ operators with $j,k\in\{1,2\}$ and $i=3$ (second column), and $i,k=3$ and $j\in\{1,2\}$ (third column).

LSP	$\mathbf{L_3Q_3D}$
$\tilde{\ell}\,(\tilde{\nu})$	$2\ell+2\tau+2t+2j_l/2\ell+\tau+t+b+2j_l+E_T^{\rm miss}/2\ell+2b+2j_l+E_T^{\rm miss}/\ell+2\tau+2t+2j_l+E_T^{\rm miss}/$ $\ell+\tau+t+b+2j_l+E_T^{\rm miss}/\ell+2b+2j_l+E_T^{\rm miss}$
$\tilde{e}$	$2\ell+2\tau+2t+2j_l/2\ell+\tau+t+b+2j_l+E_T^{\rm miss}/2\ell+2b+2j_l+E_T^{\rm miss}$
$\tilde{\tau}_L\,(\tilde{\nu}_\tau)$	$2j_l+2j_3$
$\tilde{\tau}_R$	$4\tau+2t+2j_l/3\tau+t+b+2j_l+E_T^{\rm miss}/2\tau+2b+2j_l+E_T^{\rm miss}$
$\tilde{g}$	$2\tau+2t+2j_l/\tau+t+b+2j_l+E_T^{\rm miss}$
$\tilde{q}$	$2\tau+2t+4j_l/\tau+t+b+4j_l+E_T^{\rm miss}$
$\tilde{u}$	$2\tau+2t+4j_l/\tau+t+b+4j_l+E_T^{\rm miss}$
$\tilde{d}$	$2\tau+2t/\tau+t+b+E_T^{\rm miss}$
$\tilde{t}_L(\tilde{b}_L)$	$2\tau+2j_l$
$\tilde{t}_R$	$2\tau+4t+2j_l/\tau+3t+b+2j_l+E_T^{\rm miss}$
$\tilde{b}_R$	$2\tau+2t+2b+2j_l/\tau+t+3b+2j_l+E_T^{\rm miss}$
$\tilde{B},\ \tilde{W},\ \tilde{H}$	$2\tau+2j_l+2j_3/\tau+2j_l+2j_3+E_T^{\rm miss}/2b+2j_l+E_T^{\rm miss}$

Table 10. Same as table 6 but for $L_iQ_j\bar{D}_k$ operators with $i,j=3$ and $k\in\{1,2\}$.

JHEP07(2023)215

LSP	$\mathbf{L_3Q_3D_3}$
$\tilde{\ell}\,(\tilde{\nu})$	$2\ell+2\tau+2t+2b/2\ell+\tau+t+3b+E_T^{\rm miss}/2\ell+4b+E_T^{\rm miss}/\ell+2\tau+2t+2b+E_T^{\rm miss}/$ $\ell+\tau+t+3b+E_T^{\rm miss}/\ell+4b+E_T^{\rm miss}$
$\tilde{e}$	$2\ell+2\tau+2t+2b/2\ell+\tau+t+3b+E_T^{\rm miss}/2\ell+4b+E_T^{\rm miss}$
$\tilde{\tau}_L\,(\tilde{\nu}_\tau)$	$2b+2j_3$
$\tilde{\tau}_R$	$4\tau+2t+2b/3\tau+t+3b+E_T^{\rm miss}/2\tau+4b+E_T^{\rm miss}$
$\tilde{g}$	$2\tau+2t+2b/\tau+t+3b+E_T^{\rm miss}$
$\tilde{q}$	$2\tau+2t+2b+2j_l/\tau+t+3b+2j_l+E_T^{\rm miss}$
$\tilde{u}$	$2\tau+2t+2b+2j_l/\tau+t+3b+2j_l+E_T^{\rm miss}$
$\tilde{d}$	$2\tau+2t+2b+2j_l/\tau+t+3b+2j_l+E_T^{\rm miss}$
$\tilde{t}_L(\tilde{b}_L)$	$2\tau+2b$
$\tilde{t}_R$	$2\tau+4t+2b/\tau+3t+3b+E_T^{\rm miss}$
$\tilde{b}_R$	$2\tau+2t/\tau+t+b+E_T^{\rm miss}$
$\tilde{B},\ \tilde{W},\ \tilde{H}$	$2\tau+2b+2j_3/\tau+2b+2j_3+E_T^{\rm miss}/4b+E_T^{\rm miss}$

Table 11. Same as table 6 but for $L_iQ_j\bar{D}_k$ operators with $i,j,k=3$.

4 Sample application of the framework: LLE couplings

4.1 Benchmark scenarios

We now demonstrate the practical application of our framework by using it to calculate mass bounds on SUSY particles in a wide range of RPV scenarios. Throughout this section, for simplicity, we assume that the only non-zero RPV coupling corresponds to a single $LL\bar{E}$ operator, although — as mentioned — generalization to several non-zero RPV couplings is possible by combining the different rows of our signature tables. Further, we assume all mass eigenstates are aligned with the gauge eigenstates, except for the neutral Higgsinos which are assumed to be maximally mixed.

As discussed in section 3, the signatures in our 'RPV Dictionary' have significant coverage through existing ATLAS and CMS searches, even if only indirectly. We can, therefore, reinterpret these searches in the context of RPV scenarios to set limits on the latter. In the $LL\bar{E}$ scenario, these can be comparable to or even more constraining than the MSSM limits.

In order to calculate the mass limits, we have simulated SUSY processes at leading order using the program MadGraph5_aMC@NLO [129] linked to PYTHIA 8.2 [130]. We have employed the UFO RPV-MSSM model file available at ref. [131]. The decays are computed under the narrow-width approximation. The branching ratios for two-body decays are computed by MadGraph5_aMC@NLO, while for higher-multiplicity decays — to save computational time — we set them by hand; the details of how we do this are given in section A. The width is always set by hand to a small arbitrary value (smaller than the experimental resolution) such that the decay of the LSP remains prompt; under the narrow-width approximation, the results are independent of the number. PYTHIA 8.2 then produces the

JHEP07(2023)215

LSP	Production	Coupling	LSP Decay		Label
$\tilde{g}$	Direct	λ_{121}	$2e + 2j_l + \nu_\mu$	$e + \mu + 2j_l + \nu_e$	$\mathrm{D}_{\tilde{g}}^{e\mu e}$
	Direct	λ_{121}	$2e + 2b + \nu_\mu$	$e + \mu + 2b + \nu_e$	$\mathrm{D}_{\tilde{g}}^{e\mu e-b}$
	Direct	λ_{121}	$2e + 2t + \nu_\mu$	$e + \mu + 2t + \nu_e$	$\mathrm{D}_{\tilde{g}}^{e\mu e-t}$
	Direct	λ_{122}	$2\mu + 2j_l + \nu_e$	$e + \mu + 2j_l + \nu_\mu$	$\mathrm{D}_{\tilde{g}}^{e\mu\mu}$
	Direct	λ_{311}	$2e + 2j_l + \nu_\tau$	$e + \tau + 2j_l + \nu_e$	$\mathrm{D}_{\tilde{g}}^{\tau ee}$
	Direct	λ_{313}	$2\tau + 2j_l + \nu_e$	$e + \tau + 2j_l + \nu_\tau$	$\mathrm{D}_{\tilde{g}}^{\tau e\tau}$

Table 12. Details of our benchmarks: the first two columns depict the LSP and the production mode considered, respectively; the RPV coupling assumed to be non-zero is shown in the third column; the fourth column represents the possible decays of the LSP (these are split into two columns for better readability); the last column shows the notation we use for labeling the scenario.

final decayed and showered event samples. These are passed through `CheckMATE 2` [132–136] which uses a database of several existing `ATLAS` and `CMS` analyses in order to determine whether the RPV-MSSM parameter point used to generate the event sample can be excluded or not.[10] Detector effects have been accounted for through the `DELPHES 3` [138] detector simulation module linked with `CheckMATE 2`.

We now describe the various benchmark scenarios we study. These have been designed to cover what, we believe, should be all relevant possibilities for the $LL\bar{E}$ case, subject to our minimal assumptions.

Gluino LSP. The first set of scenarios we consider is with a gluino LSP. It is sufficient to consider only direct gluino-pair production since the cross-section is higher than any channel where the gluino LSP is produced in cascade decays (see discussion in section B). Thus, in our simulation, we consider the rest of the spectrum to be decoupled; this gives us the most conservative, model-independent exclusion limits. However, we assume that, despite this decoupling, the gluino LSP still decays promptly; see section A for details on the specific decay modes chosen in the simulation. In the first three scenarios, we consider λ_{121} to be the only non-zero RPV operator. The characteristic signature for the gluino decay is $2\ell + 2j + E_T^{\mathrm{miss}}$, cf. table 2. Here j can be a light, top, or bottom jet depending on the nature of the virtual squark involved in the decay; the three scenarios target the possible dependence of the coverage on this choice. Next, to study how the results are affected if the RPV operator leads to more muons or taus instead of electrons, we consider three more scenarios corresponding to $\lambda_{122}, \lambda_{311}$, and λ_{313}, respectively, being the sole non-zero RPV couplings. The details of all gluino benchmarks have been summarized in table 12.

[10] We note that we limit ourselves to the analyses already implemented in `CheckMATE 2` as of December 2022; the list of implemented analyses can be found at ref. [137]. Some analyses explicitly targeting $LL\bar{E}$ models such as the most relevant SRs from ref. [107] are not implemented. Despite this, we observe excellent coverage.

JHEP07(2023)215

LSP	Production	Coupling	LSP Decay		Label
$\tilde{q}/\tilde{u}/\tilde{d}$	Direct $\tilde{g}$	λ_{121}	$2e + j_l + \nu_\mu$	$e + \mu + j_l + \nu_e$	$\mathrm{D}^{e\mu e}_{\tilde{q}}$ $\mathrm{I}^{e\mu e}_{\tilde{g}\to\tilde{q}}$
	Direct $\tilde{g}$	λ_{313}	$2\tau + j_l + \nu_e$	$e + \tau + j_l + \nu_\tau$	$\mathrm{D}^{\tau e\tau}_{\tilde{q}}$ $\mathrm{I}^{\tau e\tau}_{\tilde{g}\to\tilde{q}}$
$\tilde{q}_3/\tilde{t}/\tilde{b}$	Direct $\tilde{g}$	λ_{121}	$2e + j_3 + \nu_\mu$	$e + \mu + j_3 + \nu_e$	$\mathrm{D}^{e\mu e}_{\tilde{q}_3}$ $\mathrm{I}^{e\mu e}_{\tilde{g}\to\tilde{q}_3}$
	Direct $\tilde{g}$	λ_{313}	$2\tau + j_3 + \nu_e$	$e + \tau + j_3 + \nu_\tau$	$\mathrm{D}^{\tau e\tau}_{\tilde{q}_3}$ $\mathrm{I}^{\tau e\tau}_{\tilde{g}\to\tilde{q}_3}$

Table 13. As in table 12 but for the squark LSP benchmarks.

Squark LSPs. Similar to above, for squark LSP scenarios, we first consider only direct pair production with the other sparticles decoupled. Thus, we have selected two scenarios each for the light-flavor squarks ($\tilde{q}$, $\tilde{u}$, $\tilde{d}$), and the heavy-flavor ones ($\tilde{q}_3$, $\tilde{t}$, $\tilde{b}$), corresponding to the couplings λ_{121} and λ_{313}.[11] All squarks within a particular scenario are considered mass-degenerate for simplicity.

For the squarks, cascade decays involving gluino production channels (pair as well as associated) can also be relevant since these can have a higher cross-section than the direct production channels, cf. the discussion in section B. Thus, we include four more scenarios — covering the two couplings for each of the two squark groups — where the gluino and squarks are both kinematically accessible, while the rest of the spectrum is decoupled (again, in a way that the squarks still decay promptly according to branching ratios described in section A). The corresponding results are presented as two-dimensional plots in the gluino mass vs. squark mass plane. The details of all the squark benchmarks have been summarized in table 13.

Electroweakino LSPs. For the electroweakinos, we study three sets of scenarios corresponding to the winos ($\tilde{W}$), the Higgsinos ($\tilde{H}$), or the bino ($\tilde{B}$) being the LSP(s), respectively.

For the winos and the higgsinos, as before, we look at scenarios focusing on the direct modes, as well as the relevant indirect modes mentioned in section B. For winos, the latter includes production of gluinos, light-flavor squarks, or heavy-flavor squarks. However, the latter two scenarios have similar features, so we only focus on the light-flavor squarks. For the higgsinos, we include only production of gluinos and the heavy-flavor squarks since their coupling to the light-flavor squarks is suppressed.

[11] These couplings correspond to the two extreme cases: maximum and minimum number of light leptons in the final state. For the remaining scenarios we will only consider these cases; the results for the other coupling configurations can be interpolated from the gluino LSP results.

JHEP07(2023)215

For the bino, direct production is not relevant due to the small cross-section, and thus we only study indirect modes. This time, we need to consider the possibility of each of the other SUSY particles being the parent: this includes the colored sector, the winos, the Higgsinos, and the sleptons.

As before, apart from the LSP(s) and the relevant parent sparticle(s), all other SUSY fields are considered decoupled, in a way that the LSP decay remains prompt. We study scenarios corresponding to both λ_{121} and λ_{313}. The details for all benchmarks corresponding to electroweakino LSPs have been summarized in table 14.

Slepton LSPs. Finally, we have the slepton LSP scenarios. For each case — light-flavor sleptons ($\tilde{\ell}/\tilde{\nu}/\tilde{e}$), and heavy-flavor sleptons ($\tilde{\tau}_L/\tilde{\nu}_\tau/\tilde{\tau}_R$) — we study direct and indirect production, once again for the couplings λ_{121} and λ_{313}. The relevant indirect modes include every sparticle except the Bino, cf. discussion in section B. We only study scenarios with $\tilde{g}$ or $\tilde{W}$ parents; results for other colored sparticles or electroweakinos can be interpolated.

Unlike sparticles considered so far, sleptons can couple directly to the $LL\bar{E}$ operators, depending on the flavor configuration. This can significantly affect the decay modes for a given slepton. To study this effect, we also include scenarios with non-zero λ_{122} and λ_{311} for both slepton classes. The details of the slepton benchmarks are summarized in table 15.

JHEP07(2023)215

LSP	Production	Coupling	LSP Decay		Label
$\tilde{W}$	Direct				$\mathrm{D}^{e\mu e}_{\tilde{W}}$
	$\tilde{g}$	λ_{121}	$2e+\nu_\mu/2e+\mu$	$e+\mu+\nu_e/e+\nu_e+\nu_\mu$	$\mathrm{I}^{e\mu e}_{\tilde{g}\to\tilde{W}}$
	$\tilde{q}/\tilde{u}/\tilde{d}$				$\mathrm{I}^{e\mu e}_{\tilde{q}\to\tilde{W}}$
	Direct				$\mathrm{D}^{\tau e\tau}_{\tilde{W}}$
	$\tilde{g}$	λ_{313}	$2\tau+\nu_e/e+2\tau$	$e+\tau+\nu_\tau/\tau+\nu_e+\nu_\tau$	$\mathrm{I}^{\tau e\tau}_{\tilde{g}\to\tilde{W}}$
	$\tilde{q}/\tilde{u}/\tilde{d}$				$\mathrm{I}^{\tau e\tau}_{\tilde{q}\to\tilde{W}}$
$\tilde{H}$	Direct				$\mathrm{D}^{e\mu e}_{\tilde{H}}$
	$\tilde{g}$	λ_{121}	$2e+V+\nu_\mu$	$e+\mu+V+\nu_e$	$\mathrm{I}^{e\mu e}_{\tilde{g}\to\tilde{H}}$
	$\tilde{q}_3/\tilde{t}/\tilde{b}$				$\mathrm{I}^{e\mu e}_{\tilde{q}_3\to\tilde{H}}$
	Direct				$\mathrm{D}^{\tau e\tau}_{\tilde{H}}$
	$\tilde{g}$	λ_{313}	$2\tau+V+\nu_e$	$e+\tau+V+\nu_\tau$	$\mathrm{I}^{\tau e\tau}_{\tilde{g}\to\tilde{H}}$
	$\tilde{q}_3/\tilde{t}/\tilde{b}$				$\mathrm{I}^{\tau e\tau}_{\tilde{q}_3\to\tilde{H}}$
$\tilde{B}$	$\tilde{g}$				$\mathrm{I}^{e\mu e}_{\tilde{g}\to\tilde{B}}$
	$\tilde{q}/\tilde{u}/\tilde{d}$				$\mathrm{I}^{e\mu e}_{\tilde{q}\to\tilde{B}}$
	$\tilde{q}_3/\tilde{t}/\tilde{b}$				$\mathrm{I}^{e\mu e}_{\tilde{q}_3\to\tilde{B}}$
	$\tilde{\ell}/\tilde{\nu}/\tilde{e}$	λ_{121}	$2e+\nu_\mu$	$e+\mu+\nu_e$	$\mathrm{I}^{e\mu e}_{\tilde{\ell}\to\tilde{B}}$
	$\tilde{\tau}_L/\tilde{\nu}_\tau/\tilde{\tau}_R$				$\mathrm{I}^{e\mu e}_{\tilde{\tau}\to\tilde{B}}$
	$\tilde{W}$				$\mathrm{I}^{e\mu e}_{\tilde{W}\to\tilde{B}}$
	$\tilde{H}$				$\mathrm{I}^{e\mu e}_{\tilde{H}\to\tilde{B}}$
	$\tilde{g}$				$\mathrm{I}^{\tau e\tau}_{\tilde{g}\to\tilde{B}}$
	$\tilde{q}/\tilde{u}/\tilde{d}$				$\mathrm{I}^{\tau e\tau}_{\tilde{q}\to\tilde{B}}$
	$\tilde{q}_3/\tilde{t}/\tilde{b}$				$\mathrm{I}^{\tau e\tau}_{\tilde{q}_3\to\tilde{B}}$
	$\tilde{\ell}/\tilde{\nu}/\tilde{e}$	λ_{313}	$2\tau+\nu_e$	$e+\tau+\nu_\tau$	$\mathrm{I}^{\tau e\tau}_{\tilde{\ell}\to\tilde{B}}$
	$\tilde{\tau}_L/\tilde{\nu}_\tau/\tilde{\tau}_R$				$\mathrm{I}^{\tau e\tau}_{\tilde{\tau}\to\tilde{B}}$
	$\tilde{W}$				$\mathrm{I}^{\tau e\tau}_{\tilde{W}\to\tilde{B}}$
	$\tilde{H}$				$\mathrm{I}^{\tau e\tau}_{\tilde{H}\to\tilde{B}}$

Table 14. As in table 12 but for the electroweakino LSP benchmarks.

JHEP07(2023)215

LSP	Production	Coupling	LSP Decay		Label
$\tilde{\ell}/\tilde{\nu}/\tilde{e}$	Direct				$\mathrm{D}^{e\mu e}_{\tilde{\ell}}$
	$\tilde{g}$	λ_{121}	$2e/e+\mu$	$e+\nu_e/e+\nu_\mu$	$\mathrm{I}^{e\mu e}_{\tilde{g}\to\tilde{\ell}}$
	$\tilde{W}$		$\mu+\nu_e$	$*$	$\mathrm{I}^{e\mu e}_{\tilde{W}\to\tilde{\ell}}$
	Direct				$\mathrm{D}^{e\tau}_{\tilde{\ell}}$
	$\tilde{g}$	λ_{313}	$2\tau/\tau+\nu_\tau$	$*$	$\mathrm{I}^{\tau e\tau}_{\tilde{g}\to\tilde{\ell}}$
	$\tilde{W}$				$\mathrm{I}^{\tau e\tau}_{\tilde{W}\to\tilde{\ell}}$
	Direct	λ_{122}	$2\mu/e+\mu/e+\nu_\mu$	$\mu+\nu_e/\mu+\nu_\mu/*$	$\mathrm{D}^{e\mu\mu}_{\tilde{\ell}}$
	Direct	λ_{311}	$e+\tau/e+\nu_\tau$	$\tau+\nu_e/*$	$\mathrm{D}^{\tau ee}_{\tilde{\ell}}$
$\tilde{\tau}_L/\tilde{\nu}_\tau/\tilde{\tau}_R$	Direct				$\mathrm{D}^{e\mu e}_{\tilde{\tau}}$
	$\tilde{g}$	λ_{121}	$2e+\tau+\nu_\mu$	$2e+\nu_\mu+\nu_\tau$	$\mathrm{I}^{e\mu e}_{\tilde{g}\to\tilde{\tau}}$
	$\tilde{W}$		$e+\mu+\tau+\nu_e$	$e+\mu+\nu_e+\nu_\tau$	$\mathrm{I}^{e\mu e}_{\tilde{W}\to\tilde{\tau}}$
	Direct				$\mathrm{D}^{\tau e\tau}_{\tilde{\tau}}$
	$\tilde{g}$	λ_{313}	$e+\tau/e+\nu_\tau$	$\tau+\nu_e$	$\mathrm{I}^{\tau e\tau}_{\tilde{g}\to\tilde{\tau}}$
	$\tilde{W}$				$\mathrm{I}^{\tau e\tau}_{\tilde{W}\to\tilde{\tau}}$
	Direct	λ_{122}	$2\mu+\tau+\nu_e/e+\mu+\tau+\nu_\mu$	$2\mu+\nu_e+\nu_\tau/e+\mu+\nu_\mu+\nu_\tau$	$\mathrm{D}^{e\mu\mu}_{\tilde{\tau}}$
	Direct	λ_{311}	$2e/e+\nu_e$	$2e+\tau+\nu_\tau/e+2\tau+\nu_e$	$\mathrm{D}^{\tau ee}_{\tilde{\tau}}$

Table 15. As in table 12 but for the slepton LSP benchmarks. For brevity, we skip showing decay modes explicitly (indicated by $*$) for some sleptons that do not couple directly to the relevant RPV operator (e.g., $\tilde{\mu}_R$ LSP with λ_{121}). However, the details of how we include these modes in our simulations can be found in section A.

JHEP07(2023)215

Reference and search region	Representative cuts	Most sensitive for
CMS-ewk-4ℓ [44] SR **G05**	$\geq 4\ell$, $0b$, $E_T^{\rm miss}$	$D_{\tilde{g}}^{e\mu e}$, $D_{\tilde{g}}^{e\mu\mu}$, $D_{\tilde{q},\tilde{W},\tilde{H}}^{e\mu e}$, $D_{\tilde{\ell}}^{\tau ee}$, $D_{\tilde{\tau}}^{e\mu e}$, $D_{\tilde{\tau}}^{e\mu\mu}$
ATLAS-gluino-SS/3ℓ [23] SR **Rpv2L**	$\geq 2\ell$, $\geq 6j$	$D_{\tilde{g}}^{e\mu e}$, $D_{\tilde{g}}^{e\mu\mu}$, $D_{\tilde{g}}^{e\mu e-b}$, $D_{\tilde{g}}^{e\mu e-t}$, $D_{\tilde{g}}^{\tau ee}$, $D_{\tilde{q}_3}^{e\mu e}$
ATLAS-RPV-1ℓ/SS [55] SR **SS-6j100-0b**	$\geq 2\ell$, $\geq 6j$, $0b$	$D_{\tilde{g}}^{\tau ee}$, $D_{\tilde{g}}^{\tau e\tau}$, $D_{\tilde{q}}^{\tau e\tau}$
ATLAS-gluino-SS/3ℓ-1b [139] SR **Rpc3L1bH**	$\geq 3\ell$, $\geq 4j$, $\geq 1b$, $E_T^{\rm miss}$	$D_{\tilde{q}_3}^{e\mu e}$, $D_{\tilde{q}_3}^{\tau e\tau}$
CMS-ewk-2τ2ℓ [44] SR **K03**	2ℓ, 2τ, $E_T^{\rm miss}$	$D_{\tilde{W}}^{\tau e\tau}$, $D_{\tilde{H}}^{\tau e\tau}$
CMS-ewk-3ℓ [44] SR **A44**	3ℓ, $E_T^{\rm miss}$	$D_{\tilde{\ell}}^{e\mu e}$, $D_{\tilde{\ell}}^{e\mu\mu}$, $D_{\tilde{\tau}}^{\tau ee}$
CMS-ewk-1τ3ℓ [44] SR **I04**	3ℓ, 1τ, $E_T^{\rm miss}$	$D_{\tilde{\ell}}^{\tau e\tau}$
CMS-ewk-2τ1ℓ [44] SR **F12**	1ℓ, 2τ, $E_T^{\rm miss}$	$D_{\tilde{\tau}}^{\tau e\tau}$

Table 16. Summary of the most sensitive searches in our numerical simulations. The first column lists existing ATLAS and CMS searches providing sensitivity and our shorthand notation for each; the second column summarizes the relevant cuts; and the last column refers to the scenario labels presented in tables 12–15. We have color-coded the labels according to the final state topologies of section 3: $3L + E_T^{\rm miss}$, $4L + (0-4)j + E_T^{\rm miss}$, and $5L + E_T^{\rm miss}$. The same searches also constrain the $\mathrm{I}_{\tilde{x}\to\tilde{p}}$ scenarios (not shown here).

4.2 Results

Before presenting the numerical results of our simulations, we stress one important detail: even though our benchmarks correspond to simple scenarios where all sparticles other than the LSP (and NLSP) are decoupled, we expect our results to be more general. Since the characteristic signature from the LSP decay — which provides the exclusion, as we show below — is independent of the spectrum details, the sensitivity should only be slightly modified for scenarios with arbitrary sparticle mass spectra, as long as the objects in the characteristic topology do not become too soft.

We now discuss our results. All relevant details for the ATLAS and CMS searches implemented in CheckMATE 2 that show sensitivity to our scenarios have been summarized in table 16 for reference. This list is merely meant to illustrate the searches with the strongest sensitivity and is not exhaustive. When there are multiple overlapping searches offering comparable sensitivity, we have omitted some of them.

4.2.1 Direct production

Figure 2 shows a summary of the mass limits corresponding to 95% confidence level for the direct-production scenarios, i.e., all the $\mathrm{D}_{\tilde{p}}$ scenarios from tables 12–15, where $\tilde{p}$ stands for the relevant LSP. The rest of the spectrum is assumed to be decoupled in these benchmarks, while the LSP decays remain prompt. We see that the exclusion limits are comparable to the current mass bounds corresponding to the regular MSSM (see, for instance, ref. [12]). We now discuss the results in more detail in the following paragraphs.

The $\tilde{g}$-LSP scenarios can be ruled out up to about $m_{\tilde{g}} \sim 2.1 - 2.4\,\mathrm{TeV}$, with the weaker limits corresponding to cases where the λ_{ijk} coupling involves third-generation indices. The strongest limit is achieved for scenarios involving couplings to light leptons and decay via off-shell top squarks. The signature from pair production for the gluino benchmarks is $4L + 4j + E_T^{\rm miss}$. In general, the strongest sensitivity comes, as expected, from multilepton

JHEP07(2023)215

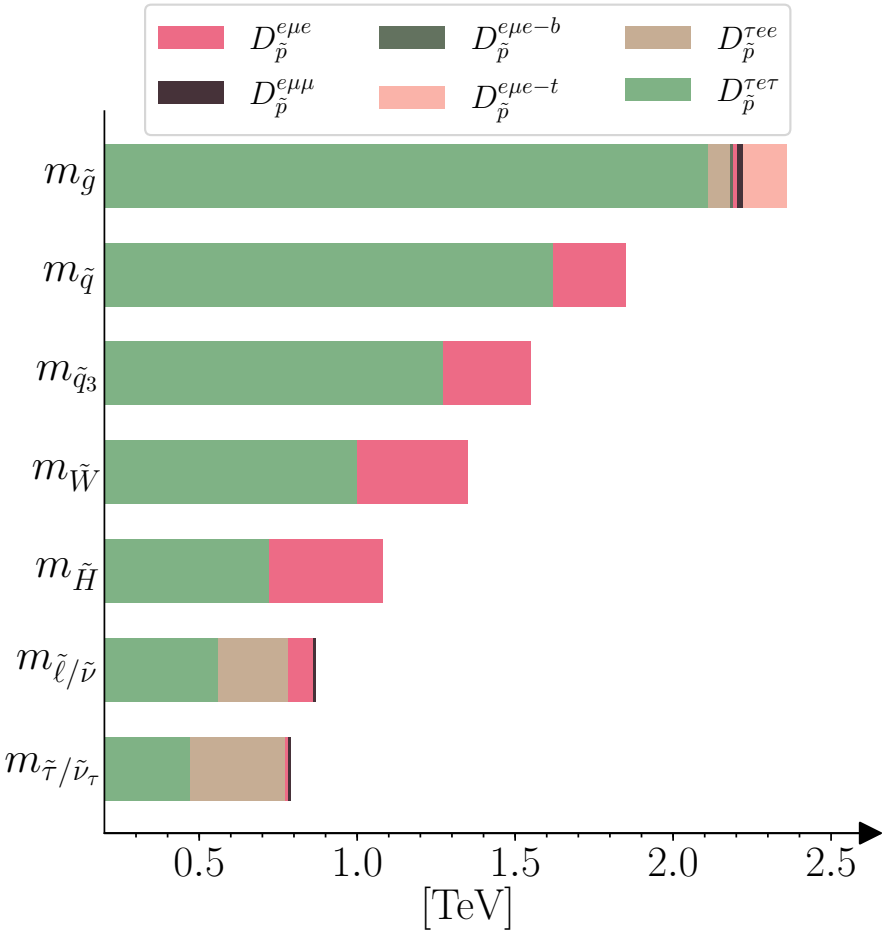

Figure 2. 95% confidence-level mass-exclusion limits for various LSPs corresponding to direct pair production. In each scenario, all sparticles other than the LSP(s) ($\tilde{p}$) are assumed to be decoupled, while the LSP decays are still prompt.

searches, especially `CMS-ewk-4`ℓ and `ATLAS-gluino-SS/3`ℓ.[12] In scenarios with heavy-flavor squarks, $\mathrm{D}^{e\mu e-b}_{\tilde{g}}$ and $\mathrm{D}^{e\mu e-t}_{\tilde{g}}$, `CMS-ewk-4`$\ell$ shows a weaker sensitivity due to the veto of b-jets. Finally, for couplings that involve τ leptons, $\mathrm{D}^{\tau ee}_{\tilde{g}}$ and $\mathrm{D}^{\tau e\tau}_{\tilde{g}}$, the most relevant analyses are `ATLAS-gluino-SS/3`ℓ and `ATLAS-RPV-1`ℓ`/SS`. Both searches offer sensitivity despite the fact that they focus only on light leptons. This is due to the fraction of gluino decays into electrons (cf. table 12), and the leptonic decay of taus. The hadronic decays of taus are reconstructed as additional jets which satisfy the jet multiplicity requirement of both searches. None of the searches are optimized for our signal but they still provide great sensitivity.

For the squarks and the electroweakinos, the final states are similar to the gluino case, albeit with fewer jets: $4L + (0-2)j + E_T^{\mathrm{miss}}$. The most stringent limits for the $\mathrm{D}^{e\mu e}_{\tilde{p}}$ scenarios are provided by `CMS-ewk-4`ℓ: $m_{\tilde{q}} \gtrsim 1.85\,\mathrm{TeV}$, $m_{\tilde{W}} \gtrsim 1.35\,\mathrm{TeV}$, $m_{\tilde{H}} \gtrsim 1.1\,\mathrm{TeV}$. The reduced jet multiplicity limits the sensitivity of `ATLAS-gluino-SS/3`ℓ and `ATLAS-RPV-1`ℓ`/SS`. The $\mathrm{D}^{\tau e\tau}_{\tilde{W}}$ and $\mathrm{D}^{\tau e\tau}_{\tilde{H}}$ scenarios are now instead covered by `CMS-ewk-2`$\tau 2\ell$,

[12] See table 16 for the notation we employ for searches.

JHEP07(2023)215

a search explicitly targeting two hadronic taus, leading to the limits, $m_{\tilde{W}} \gtrsim 1\,\text{TeV}$ and $m_{\tilde{H}} \gtrsim 720\,\text{GeV}$. However, similar to the gluino case, `ATLAS-RPV-1ℓ/SS` is the most sensitive for $\text{D}_{\tilde{q}}^{\tau e\tau}$ and rules out this scenario up to $m_{\tilde{q}} \approx 1.6\,\text{TeV}$.

The production of stops and sbottoms is special due to the presence of additional b jets, which are vetoed by `CMS-ewk-4ℓ` and `ATLAS-RPV-1ℓ/SS`. Thus, the best limits in this case come from `ATLAS-gluino-SS/3ℓ-1b` and `ATLAS-gluino-SS/3ℓ` for $\text{D}_{\tilde{q}_3}^{e\mu e}$ ($m_{\tilde{q}_3} \gtrsim 1.55\,\text{TeV}$) and $\text{D}_{\tilde{q}_3}^{\tau e\tau}$ ($m_{\tilde{q}_3} \gtrsim 1.3\,\text{TeV}$).

Finally, we have the slepton-LSP scenarios. For $\tilde{\ell}/\tilde{\nu}/\tilde{e}$, the exclusion limits lie in the broad range $m_{\tilde{\ell}} \sim 560 - 860\,\text{GeV}$. The most constraining search for scenarios $D_{\tilde{\ell}}^{e\mu e}$ and $D_{\tilde{\ell}}^{e\mu\mu}$ turns out to be `CMS-ewk-3ℓ`. This search matches the $3L + E_T^{\text{miss}}$ topology from $\tilde{\ell}\tilde{\nu}$ production, as listed in table 2. For scenarios $D_{\tilde{\ell}}^{\tau ee}$ and $D_{\tilde{\ell}}^{\tau e\tau}$, the most relevant searches are `CMS-ewk-4ℓ` and `CMS-ewk-1τ3ℓ`, respectively. The latter needs at least three light leptons and at least one hadronic tau.

In the case of $\tilde{\tau}_L/\tilde{\nu}_\tau/\tilde{\tau}_R$, a large gap in sensitivity is observed between scenarios $D_{\tilde{\tau}}^{e\mu e}$, $D_{\tilde{\tau}}^{e\mu\mu}$, and $D_{\tilde{\tau}}^{\tau ee}$ which are excluded up to $m_{\tilde{\tau}} \sim 780 - 790\,\text{GeV}$; and the $D_{\tilde{\tau}}^{\tau e\tau}$ scenario with a reach of just $m_{\tilde{\tau}} \gtrsim 470\,\text{GeV}$. The former are covered by `CMS-ewk-4ℓ` and `CMS-ewk-3ℓ`, while the latter is targeted by `CMS-ewk-2τ1ℓ`. The topologies targeted by all the above search regions match those in tables 2–3.

4.2.2 Cascade decays

We next look at the results for the indirect-production/cascade-decay scenarios, i.e., all the $\text{I}_{\tilde{x}\to\tilde{p}}$ benchmarks from tables 12–15, where $\tilde{p}$ is the LSP and $\tilde{x}$ denotes the directly produced parent particle decaying into the LSP. Cascade decays are especially important for scenarios with a bino LSP, where direct production is irrelevant. For all other LSP types, the limits from direct LSP production (corresponding to $D_{\tilde{p}}$) are also taken into account.

In general, exclusion limits are mostly independent of the LSP mass (with a few exceptions) as the signal regions have high acceptance and the limit is driven by the production cross-section. A loss in sensitivity is observed in regions with small mass splittings only for models where the most sensitive signal region requires additional jets. In the bino scenarios, a loss in sensitivity is also observed for low LSP masses as its decay products carry energies that are too low to survive the search region cuts. This effect is not observed for other scenarios as the direct production of LSP becomes dominant for lower masses.

Squark LSPs. In figure 3, we show the exclusion limits for $\tilde{q}/\tilde{u}/\tilde{d}$-LSPs (figure 3a) and $\tilde{q}_3/\tilde{t}/\tilde{b}$-LSPs (figure 3b) for a non-decoupled gluino. The relevant production processes are gluino-gluino, squark-squark, and associated gluino-squark production, followed by the decay of the gluino into the squark LSP(s) and a jet, and finally the LSP decay via the RPV operator into $2L + j + E_T^{\text{miss}}$.[13] The phase-space region $m_{\tilde{g}} < m_{\tilde{q}}$ ($m_{\tilde{g}} < m_{\tilde{q}_3} + m_t$) is kinematically disallowed[14] in the light-flavor (heavy-flavor) scenario, where we have

[13] See section A for a detailed discussion on the specific decay modes we pick for each simulation.

[14] Technically, for the heavy-flavor scenario, the region $m_{\tilde{q}_3} \leq m_{\tilde{g}} < m_{\tilde{q}_3} + m_t$ lets the gluino decay into a sbottom (ignoring the b-quark mass), and is allowed. However, for simplicity, we will ignore this here.

JHEP07(2023)215

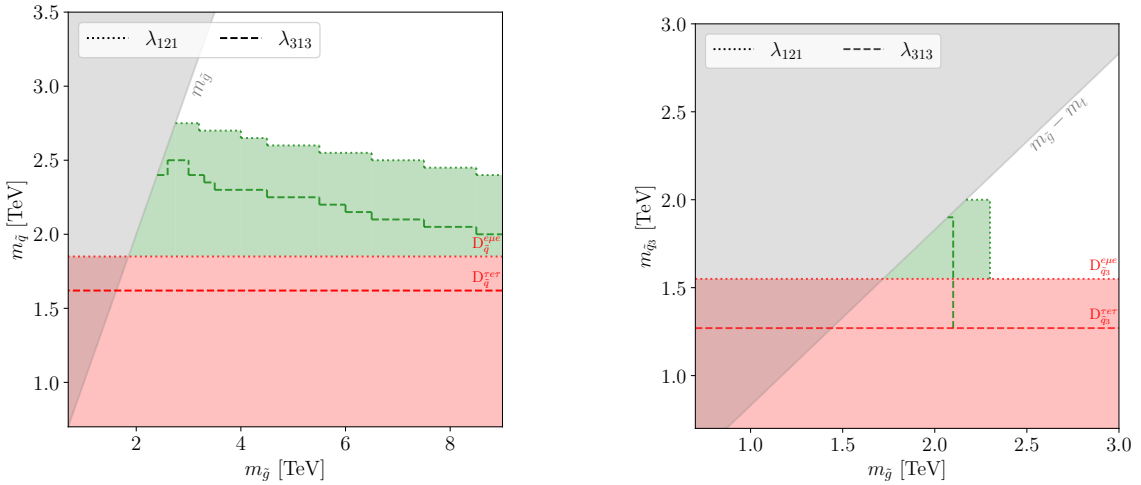

(a) $\tilde{q}/\tilde{u}/\tilde{d}$-LSPs with non-decoupled $\tilde{g}$.

(b) $\tilde{q}_3/\tilde{t}/\tilde{b}$-LSPs with non-decoupled $\tilde{g}$.

Figure 3. Exclusion regions (in green) corresponding to 95% confidence level for the $I_{\tilde{g}\to\tilde{q}}$ (left) and $I_{\tilde{g}\to\tilde{q}_3}$ (right) scenarios. The bounds of figure 2 from direct squark production also apply to the scenario and are shown in red. The gray region is kinematically disallowed in the scenario. The dotted (dashed) contours correspond to coupling λ_{121} (λ_{313}).

neglected the masses of all SM fermions except the top quark. These regions are depicted in gray in the plot.

From figure 3a, we see that $I_{\tilde{g}\to\tilde{q}}$ can be excluded roughly up to the kinematic limit as long as we are below the threshold for $\tilde{g}\tilde{g}$ production, cf. figure 2. However, even above this threshold, we can exclude large regions of the parameter space that lie beyond the bounds from direct squark-pair production with a decoupled gluino. For instance, we see that even with $m_{\tilde{g}} \sim 8\,\text{TeV}$, we get higher exclusion in the squark mass compared to the limit coming from $D_{\tilde{q}}$ (shown in red in the figure). This is due to two reasons. First, the associated-production channel (involving a single gluino) can stay kinematically accessible for longer. More importantly, a non-decoupled gluino significantly boosts direct squark-pair production cross-sections through its t-channel contributions [140]. For very high masses, the gluino is essentially decoupled and the limits start converging, i.e., the scenarios reduce to the $D_{\tilde{q}}$ cases.

For figure 3b, the exclusion limits behave differently. For both couplings, roughly all kinematically viable regions can be excluded up to the corresponding $m_{\tilde{g}}$ limits of figure 2. However, the limits reduce sharply to the $D_{\tilde{q}_3}$ bounds beyond this. For third-generation squarks, associated production as well as the boost in squark-squark cross-sections due to non-decoupled gluinos are suppressed by the small parton distribution functions (PDFs) for the heavy quarks inside the proton. Thus, as soon as gluino-pair production becomes kinematically inaccessible, the scenarios reduce to the $D_{\tilde{q}_3}$ cases.

Electroweakino LSPs. We next show the results for wino-LSP production with a non-decoupled gluino in figure 4a and non-decoupled light-flavor squarks in figure 4b.

For the gluino case, we see features similar to figure 3b. For both couplings, all phase-

JHEP07(2023)215

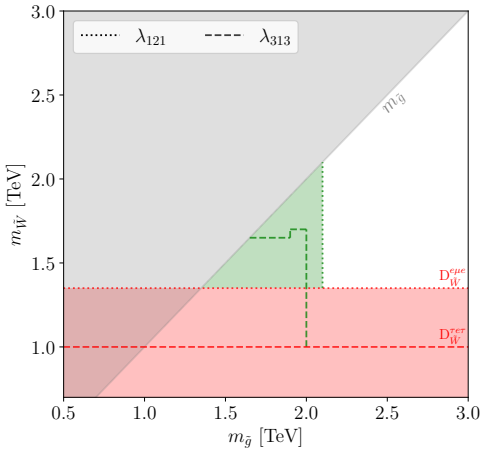

(a) $\tilde{W}$ LSP with non-decoupled $\tilde{g}$.

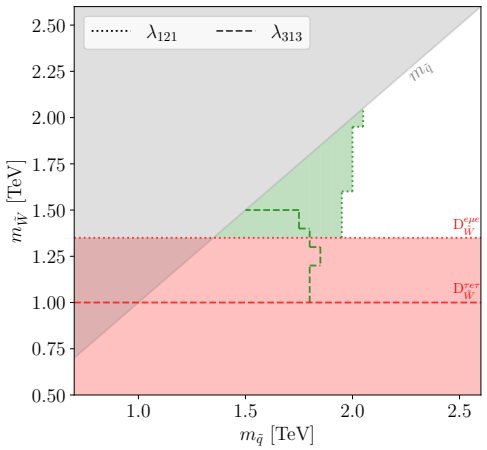

(b) $\tilde{W}$ LSP with non-decoupled $\tilde{q}/\tilde{u}/\tilde{d}$.

Figure 4. As in figure 3 but for the $I_{\tilde{g}\to\tilde{W}}$ (left) and $I_{\tilde{q}\to\tilde{W}}$ (right) scenarios.

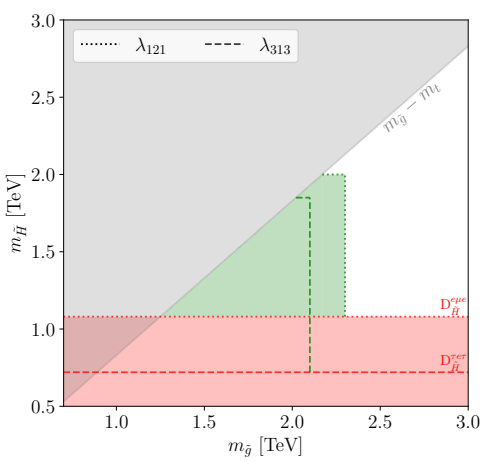

(a) $\tilde{H}$ LSP with non-decoupled $\tilde{g}$.

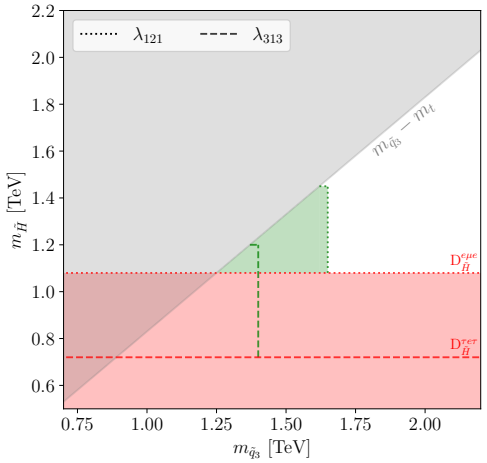

(b) $\tilde{H}$ LSP with non-decoupled $\tilde{q}_3/\tilde{t}/\tilde{b}$.

Figure 5. As in figure 3 but for the $I_{\tilde{g}\to\tilde{H}}$ (left) and $I_{\tilde{q}_3\to\tilde{H}}$ (right) scenarios.

space regions almost up to the gluino-pair production threshold can be ruled out. Beyond this, the results from $D_{\tilde{W}}$ apply. One interesting feature is the flattening of the exclusion contour for λ_{313} at $m_{\tilde{W}} \sim 1.7\,\text{TeV}$ for gluino masses, $m_{\tilde{g}} \sim 1.7 - 2\,\text{TeV}$. This reduction in sensitivity occurs because the cuts in `ATLAS-RPV-1ℓ/SS` place a high demand on the transverse momentum of the six required jets, $p_{\text{T}} > 100\,\text{GeV}$. If the wino and gluino are too close in mass, the jets produced in the gauge decay of the latter may not pass these requirements.

Figure 4b is more interesting. We again see that the parameter space roughly up to the squark-production thresholds can be ruled out and we observe the flattening effect mentioned above. However, we also see a new effect. The exclusion limit slightly weakens as we move lower in wino mass. This is clearly seen for the λ_{121} case but the reduction in sensitivity occurs for both couplings throughout the phase space. This is because squark-

JHEP07(2023)215

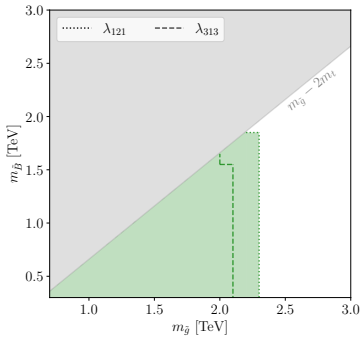

(a) $\tilde{B}$ LSP with non-decoupled $\tilde{g}$.

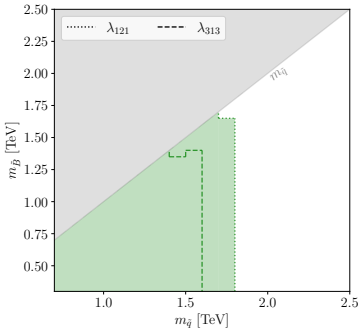

(b) $\tilde{B}$ LSP with non-decoupled $\tilde{q}/\tilde{u}/\tilde{d}$.

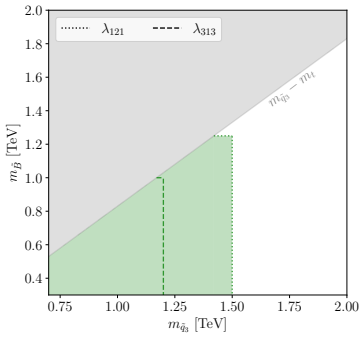

(c) $\tilde{B}$ LSP with non-decoupled $\tilde{q}_3/\tilde{t}/\tilde{b}$.

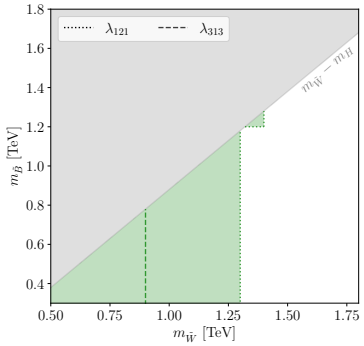

(d) $\tilde{B}$ LSP with non-decoupled $\tilde{W}$.

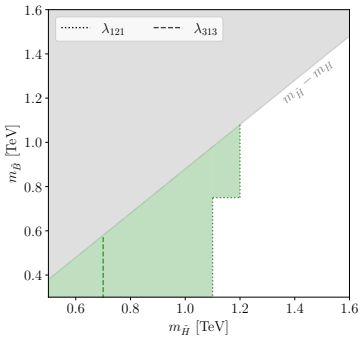

(e) $\tilde{B}$ LSP with non-decoupled $\tilde{H}$.

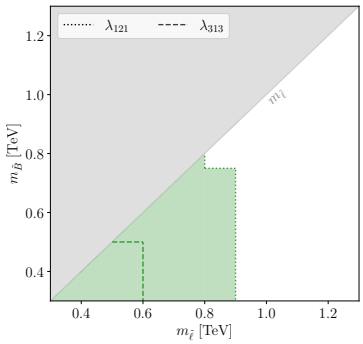

(f) $\tilde{B}$ LSP with non-decoupled $\tilde{\ell}/\tilde{\nu}/\tilde{e}$.

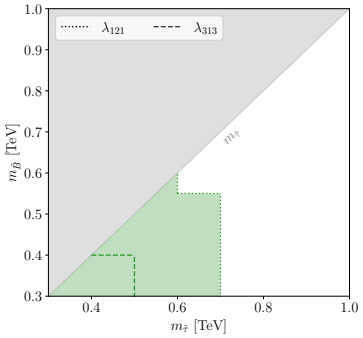

(g) $\tilde{B}$ LSP with non-decoupled $\tilde{\tau}_L/\tilde{\nu}_\tau/\tilde{\tau}_R$.

Figure 6. As in figure 3 but for the $I_{\tilde{x}\to\tilde{B}}$ scenarios.

pair production can also occur via t-channel wino exchange which can interfere negatively with the QCD contribution [141]; this interference term is bigger for lighter winos.

Next, we show the Higgsino-LSP results for non-decoupled gluinos and non-decoupled third-generation squarks in figure 5a and figure 5b, respectively. The exclusion limits show features similar to the earlier cases and are straightforward to interpret. Beyond the pair-production thresholds for the parents, the benchmarks reduce to the respective $D_{\tilde{H}}$ scenarios.

JHEP07(2023)215

The bino-LSP results are depicted in figure 6: these correspond to scenarios with gluinos (figure 6a), light-flavor squarks (figure 6b), heavy-flavor squarks (figure 6c), winos (figure 6d), Higgsinos (figure 6e), light-flavor sleptons (figure 6f), and third-generation sleptons (figure 6g). Generally, the exclusion limits cover almost the whole phase-space region up to the kinematic thresholds for the pair-production of the parents. However, there are a couple of features worth mentioning. First, we see the flattening effect, that we had described for figure 4, in scenarios $I^{\tau e\tau}_{\tilde{x}\to\tilde{B}}$ with $\tilde{x} = \tilde{q}, \tilde{\ell}, \tilde{\tau}$. The other interesting effect is the slight increase in sensitivity as the $\tilde{B}$ mass increases from very low masses to higher values. This effect can be most clearly seen in figure 6e but is a general feature in the other $\tilde{B}$ plots too. This happens due to the reason mentioned at the beginning of this subsection: for very low bino masses, the decay products are not energetic enough to pass the cuts of the analyses. We did not encounter it in the case of the other LSPs since the mass scales there were higher.

Slepton LSPs. Finally, we show the slepton-LSP results in figure 7. The exclusion limits can extend significantly in the cascade decay due to the much higher production cross-sections of other parent particles compared to direct slepton production.

LSP summary. To summarize, we collect, in figure 8, the minimum excluded mass for each sparticle, $\tilde{p}$, undergoing a cascade decay (i.e., the minimum limits obtained for each of the $\mathrm{I}_{\tilde{p}\to\tilde{x}}$ scenarios with $\tilde{x}$ the various LSPs), and compare it to the limit obtained from direct production of the sparticle when it is the LSP (i.e., the corresponding $\mathrm{D}_{\tilde{p}}$ scenarios). It is interesting to note that, although cascade decays generally lead to final states with more visible objects, the sensitivity can be both degraded or improved. The reduction in E_T^{miss} and the distribution of energy across more decay products can reduce the sensitivity. For example, the decay to a slepton or bino LSP yields in most cases the worst limits given that intermediate particles in the decay chain can become soft for compressed spectra, e.g., $\tilde{g} \to 2j + \ell + \tilde{\ell}(\to \ell\nu)$. However, changes in the decay modes due to the varying nature of the LSP can also lead to a higher number of leptons or third-generation quarks which leads to an improvement in the limits. It is worth highlighting that the degradation is around 20% at maximum, and the exclusion limits remain for all sparticles under all variations of LSP hypotheses, LSP masses, and coupling choice.

JHEP07(2023)215

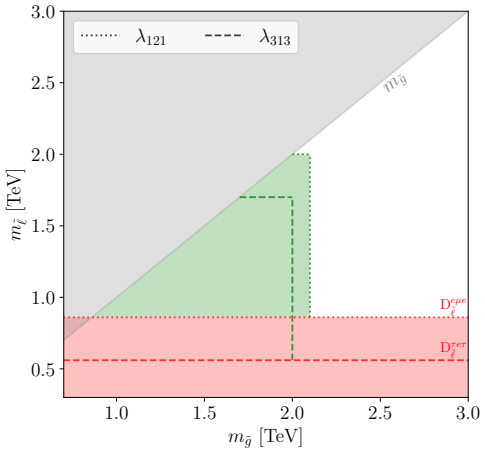

(a) $\tilde{\ell}/\tilde{\nu}/\tilde{e}$ LSPs with non-decoupled $\tilde{g}$.

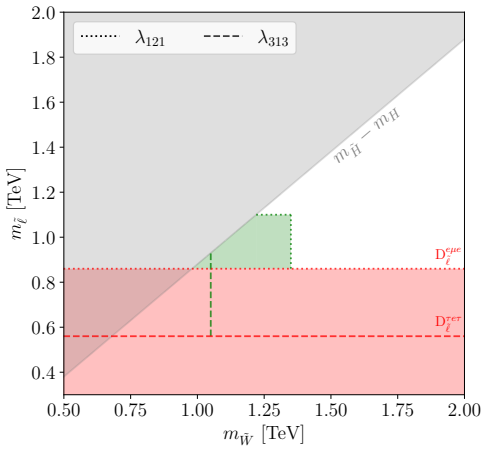

(b) $\tilde{\ell}/\tilde{\nu}/\tilde{e}$ LSPs with non-decoupled $\tilde{W}$.

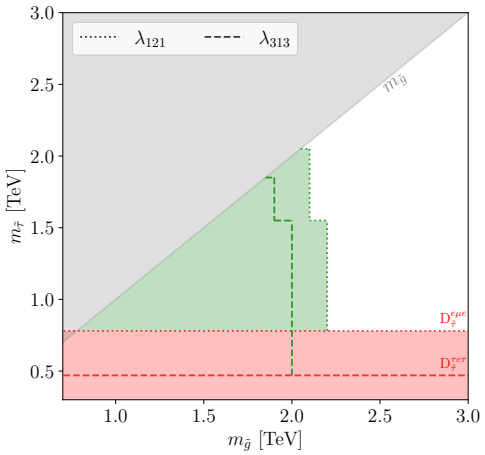

(c) $\tilde{\tau}_L/\tilde{\nu}_\tau/\tilde{\tau}_R$ LSPs with non-decoupled $\tilde{g}$.

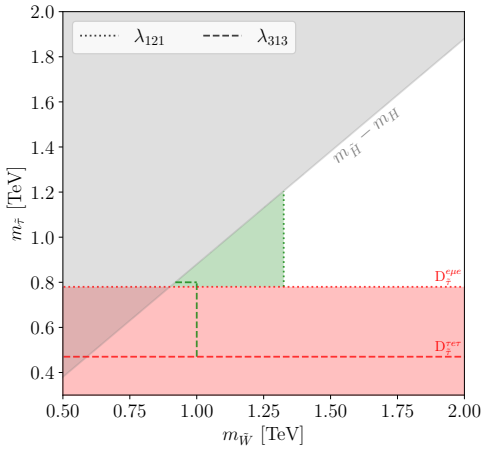

(d) $\tilde{\tau}_L/\tilde{\nu}_\tau/\tilde{\tau}_R$ LSPs with non-decoupled $\tilde{W}$.

Figure 7. As in figure 3 but for the $I_{\tilde{x}\to\tilde{\ell}/\tilde{\tau}}$ scenarios.

JHEP07(2023)215

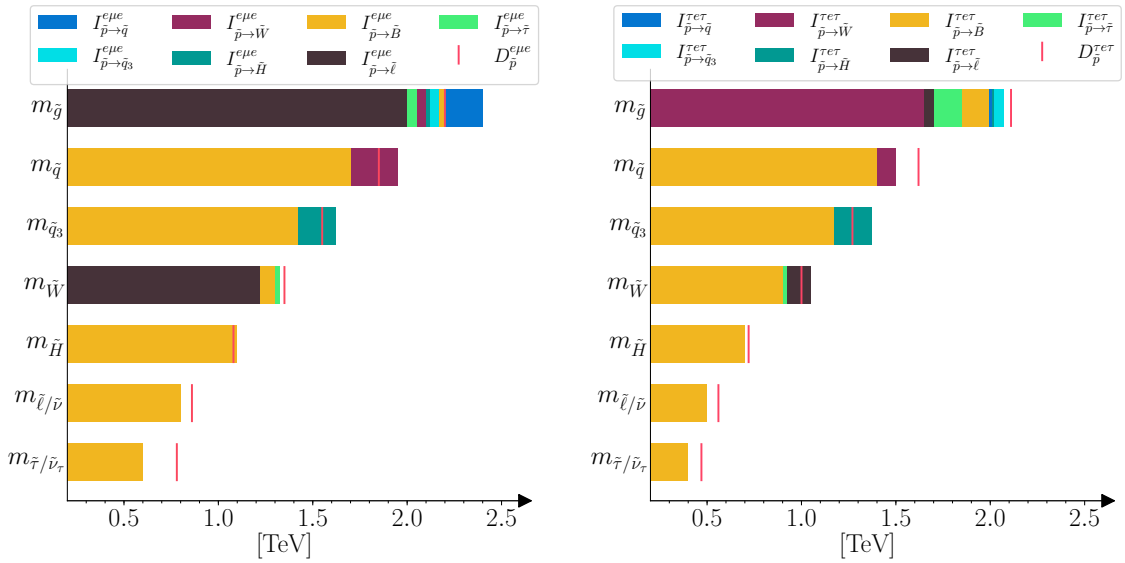

(a) λ_{121}. **(b)** λ_{313}.

Figure 8. Summary of minimum mass bounds on sparticle $\tilde{p}$ across the various $\mathrm{I}_{\tilde{p}\to\tilde{x}}$ benchmarks considered, where $\tilde{x}$ corresponds to the LSPs. The vertical red line represents the direct production mass bound when $\tilde{p}$ is the LSP, i.e., the limit corresponding to $\mathrm{D}_{\tilde{p}}$.

JHEP07(2023)215

5 Conclusions and outlook

In this paper, we have systematically analyzed the RPV-MSSM and classified the possible signatures at the LHC with the goal of compiling a minimal set of experimental searches that provides complete coverage. Our study provides, for the first time, a completely general and model-independent treatment of the phenomenology, for the case of small RPV couplings. We briefly summarize the central results of the paper:

- As demonstrated, the phenomenological space for the most general RPV-MSSM setup is vast and complicated. Nevertheless, we have shown that just 17 final state topologies (six for $LL\bar{E}$, five for $\bar{U}\bar{D}\bar{D}$, and six for $LQ\bar{D}$) are sufficient to provide complete coverage for the RPV-MSSM at the LHC; we call this the 'RPV Dictionary'. Our signature tables can be generated by using the accompanying `abc-rpv` Python library, described in section C.

- Using the 'RPV Dictionary', we have analyzed the current coverage of the RPV-MSSM at the LHC. In general, we find that even though most RPV scenarios have not been searched for directly, the vast landscape of searches implemented by `ATLAS` and `CMS` provides full coverage of the possible RPV-MSSM signatures.

- However, we do point out the need for strong experimental improvements in some of the final states in order to achieve sensitivity to electroweak production cross-sections. Some examples are found for $LQ\bar{D}$ and $U\bar{D}\bar{D}$ decays, such as $\tilde{\ell} \to jj$, $\tilde{\chi}_1^0 \to jb\nu$, and $\tilde{\chi}_1^0 \to jjj$.

- As an application of our framework, and in order to demonstrate the second point above, we have performed numerical simulations specifically for the case of a dominant $LL\bar{E}$ operator (single non-zero coupling at a time), in order to quantitively assess the coverage. We have derived mass bounds on SUSY particles within several RPV benchmark models corresponding to all relevant LSPs. We find that strong exclusion limits comparable to, or even better than, the RPC-MSSM are obtained, and these are robust across the wide range of models. Apart from clarifying the current status of several of these scenarios for which there are no explicit exclusion limits in the literature, our numerical examples demonstrate that our approach of using just a few characteristic topologies to cover the most general RPV-MSSM setting is not merely a reductionist fantasy, but can indeed offer a viable, model-independent search strategy. We have left the detailed analyses of the $LQ\bar{D}$ and $\bar{U}\bar{D}\bar{D}$ cases for future work.

We stress that there are a couple of limitations of our framework. As mentioned in the main body, we require that all decays in the cascade chain are prompt, including that of the LSP. Furthermore, we require that the final state decay products of the LSP are not too soft to be detected. This assumption is crucial and restricts us to scenarios with $m_{\text{LSP}} > \mathcal{O}(200\,\text{GeV})$. Further, while we require the RPV coupling to be large enough to cause the LSP to decay promptly, it cannot be too large, as that would modify the pattern of the cascade decays. Similarly, adding exotic particles to the MSSM spectrum that can

JHEP07(2023)215

modify the sparticle decay chains also affects our analysis. In such cases, our classification may not apply anymore. The most important restriction is that our approach — in prioritizing model independence — compromises on search sensitivity for certain scenarios. For example, if the colored sector is always kinematically accessible at the LHC, stricter bounds can be obtained by including the cascade decay products in the search signature, whereas, in our approach, we only target decay products from the LSP. The former approach is usually adopted by ATLAS and CMS in their searches for specific RPV-SUSY scenarios.

On the other hand, we believe our unbiased approach is highly relevant, given that no supersymmetry has yet been discovered at the LHC, and with the HL-LHC era just around the corner. Nevertheless, we have compiled auxiliary tables in section B that can help in designing optimized search strategies in exchange for some model-independence.

As a continuation of this work, we shall pursue a detailed numerical treatment of the $LQ\bar{D}$ and $\bar{U}\bar{D}\bar{D}$ scenarios analogous to the $LL\bar{E}$ case considered in this paper. In those cases, present coverage is less comprehensive and it is important to identify potential gaps. Furthermore, we would like to extend the present work to a systematic study of the large RPV coupling case, affecting both production and decay.

Acknowledgments

VML is funded by grant María Zambrano UP2021-044 (ZA2021-081) funded by Ministerio de Universidades and "European Union-NextGenerationEU/PRTR" and thanks support from the Spanish grants PID2020-113775GB-I00 (AEI/10.13039/501100011033) and CIPROM/2021/054 (Generalitat Valenciana). JMB is funded by grant RYC2021-030944-I funded by MCIN/AEI/10.13039/501100011033 and by the European Union NextGenerationEU/PRTR. NS is supported by the U.S. Department of Energy, Office of Science, Office of High Energy Physics under Award Number DE-SC0011845.

A Decay modes for numerical simulations

We discuss the details of the decay modes used in the numerical simulations here. As mentioned in section 4, all two-body decays are computed using MadGraph5_aMC@NLO; we only discuss the higher-body decays that we set by hand here.

Gluino LSP benchmarks. For a given coupling, λ_{iki} with $i, k \in \{1, 2, 3\}$, we assume the chain: $\tilde{g} \to (\tilde{q}/\tilde{q}_3)^* + j \to \tilde{B}^* + 2j \to 2L + E_T^{\rm miss} + 2j$, where $2L = \{L_i^+ + L_i^-\}, \{L_i^+ + L_k^-\}, \{L_k^+ + L_i^-\}$, and we set the corresponding branching ratios (BRs) to be 0.5, 0.25, and 0.25, respectively. In the above, the asterisk denotes off-shell particles, and the nature of the (s)quark is fixed by the scenario considered. We stress that the chosen decay chain and BRs represent a non-trivial choice to facilitate numerical computation; alternate choices are possible — e.g., the bino can be replaced by a wino or one flavor of slepton can be decoupled, thus, affecting the BRs. That is, we take the perspective where the branching ratios are taken to be the free variables, rather than the sparticle masses. Apart from being a simpler approach, this also saves computational time since we no longer need to

JHEP07(2023)215

calculate complicated high-multiplicity decays. Even with alternate BR choices, we expect the general implications of our results to hold.

Squark LSP benchmarks. This is very similar to the above. For a coupling λ_{iki}, we assume the decay chain for the squarks to be: $(\tilde{q}/\tilde{q}_3)^* \to \tilde{B}^* + j \to 2L + E_T^{\rm miss} + j$, where $2L = \{L_i^+ + L_i^-\}, \{L_i^+ + L_k^-\}, \{L_k^+ + L_i^-\}$, and the BRs are set to 0.5, 0.25, and 0.25, respectively.

Electroweakino LSP benchmarks.

- $\mathrm{D}_{\tilde{W}}$: the neutral wino decays as: $\tilde{W}^0 \to 2L + E_T^{\rm miss}$, for a coupling λ_{iki}, where $2L = \{L_i^+ + L_i^-\}, \{L_i^+ + L_k^-\}, \{L_k^+ + L_i^-\}$. We set the corresponding BRs to 0.5, 0.25, and 0.25, respectively. For the charged wino, we have the decay modes: $\tilde{W}^+ \to \{L_i^+ + L_i^- + L_k^+\}, \{L_i^+ + L_i^+ + L_k^-\}, \{L_i^+ + E_T^{\rm miss}\}, \{L_k^+ + E_T^{\rm miss}\}$ (analogous for $\tilde{W}^-$). We set the BR to 0.25 for each mode.

- $\mathrm{I}_{\tilde{g}\to\tilde{W}}$: the gluino decays as: $\tilde{g} \to \tilde{q}^* + j_l \to \tilde{W} + 2j_l$.

- $\mathrm{I}_{\tilde{q}\to\tilde{W}}$: the (singlet) squarks decay as: $\tilde{u}/\tilde{d} \to \tilde{g}^* + j_l \to \tilde{q}^* + 2j_l \to \tilde{W} + 3j_l$.

- $\mathrm{D}_{\tilde{H}}$: the neutral Higgsinos decay as: $\tilde{H}^0_{1(2)} \to \tilde{B}^* + Z(h) \to 2L + E_T^{\rm miss} + Z(h)$, for a coupling λ_{iki}, where $2L = \{L_i^+ + L_i^-\}, \{L_i^+ + L_k^-\}, \{L_k^+ + L_i^-\}$, with the BRs fixed to 0.5, 0.25, and 0.25, respectively. The case for $\tilde{H}^\pm$ is analogous, with $Z(h)$ replaced by $W^\pm$.

- $\mathrm{I}_{\tilde{g}\to\tilde{H}}$: here, the gluino is assumed to decay as: $\tilde{g} \to \tilde{q_3}^* + j_3 \to \tilde{H} + 2j_3$.

- In all $\tilde{B}$ LSP scenarios, the bino decays as: $\tilde{B} \to 2L + E_T^{\rm miss}$, for a coupling λ_{iki}, where $2L = \{L_i^+ + L_i^-\}, \{L_i^+ + L_k^-\}, \{L_k^+ + L_i^-\}$, with the BRs set to 0.5, 0.25, and 0.25, respectively.

- $\mathrm{I}_{\tilde{g}\to\tilde{B}}$: the gluino is assumed to decay as: $\tilde{g} \to \tilde{q_3}^* + j_3 \to \tilde{B} + 2j_3$.

Slepton LSP benchmarks.

- For all $\mathrm{D}_{\tilde{L}}$ scenarios, if a particular lepton does not couple directly to the considered operator, the decay is assumed to proceed via an off-shell bino, e.g., $\tilde{\mu}_R \to \tilde{B}^* + \mu \to 2L + \mu + E_T^{\rm miss}$, where $2L = \{L_i^+ + L_i^-\}, \{L_i^+ + L_k^-\}, \{L_k^+ + L_i^-\}$ (for a coupling λ_{iki}). The corresponding BRs are set to 0.5, 0.25, and 0.25, respectively; and so on.

- $\mathrm{I}_{\tilde{g}\to\tilde{L}}$: the gluino is assumed to decay as: $\tilde{g} \to \tilde{q}^* + j_l \to \tilde{B}^* + 2j_l \to \tilde{L} + 2j_l + L$. Here, $\tilde{L}$ refers to all the sleptons.

- $\mathrm{I}_{\tilde{W}\to\tilde{L}}$: we assume that the only contributing decays are the two-body decay modes of the wino into the left-handed sleptons; we set the decay widths of the modes into the right-handed sleptons to be zero. This can occur if, for instance, any virtual mediators that can lead to such a decay are completely decoupled.

JHEP07(2023)215

B Auxiliary tables

B.1 Production table

While compiling the 'RPV Dictionary' in section 3, we have taken a model-independent approach. In order to completely cover the RPV-MSSM landscape (within our framework assumptions), it is necessary to perform the searches compiled in tables 2–11. Often, however, one is not interested in being completely general but may have a bias for certain classes of models. For instance, it is usual in the literature to focus on scenarios where a given LSP is produced at the LHC in cascade decays of the colored sparticles; scenarios where all sparticles other than the LSP are completely decoupled are less common. Given such a bias, one can optimize the 'RPV Dictionary' by adding the objects that would arise from such cascades.

In order to facilitate the inclusion of the above, table 17 provides a list of the objects that arise in cascade-decays for each relevant production mode for each LSP. For instance, with a gluino LSP, the only relevant mode is gluino-pair production since every other channel will have a lower cross-section. For squark LSP(s), however, squark-pair, gluino-pair, and associated production are all relevant since the latter two contribute with high cross-sections when a gluino is not decoupled. Table 17 shows that the cascade to the LSP from gluino-pair (associated-pair) production leads to 2 extra jets (1 extra jet). These can then be used to optimize searches for models with squark LSPs and non-decoupled gluinos by adding the extra jet(s) to the relevant squark LSP signatures in tables 2–11. We note that each value in the table represents the maximal set of objects that is *guaranteed to arise* in the cascade without knowing the details of the spectrum; however, more objects can always be present in specific scenarios. Further, to be economical, we have grouped left-handed and right-handed sparticles into one category but it is straightforward to expand them out.

B.2 Flavor, sign configurations of leptons

Here, we compile tables that show the possible flavor and sign combinations of the leptons in the signatures of tables 2–11. In all the tables below, the indices $i, j, k \in \{1, 2, 3\}$, while the indices $a, b \in \{1, 2\}$; $\tilde{\ell}_3$ denotes a τ. For each listed configuration, the charge conjugated state (if different) is also possible but we omit listing it explicitly.

LLE signatures. The flavor and sign combinations of the leptons corresponding to the various $LL\bar{E}$ topologies are shown in table 18 ($2L + E_T^{\text{miss}}$); table 19 ($3L + E_T^{\text{miss}}$); table 20 ($4L$); table 21 ($4L + (0-4)j + E_T^{\text{miss}}$); table 22 ($5L + E_T^{\text{miss}}$); and table 23 ($6L + E_T^{\text{miss}}$). The combinations corresponding to $\tilde{B}$ also apply to the Higgsino and all colored-sector LSPs.

UDD tables. For the $\bar{U}\bar{D}\bar{D}$ topologies, the possible combinations are shown in table 24 ($1L + 2j_l + 4j + E_T^{\text{miss}}$); and table 25 ($2L + 2j_l + 4j$).

LQD tables. Finally, for the $LQ\bar{D}$ topologies, the possible configurations are shown in table 26 ($1L + (2-6)j + E_T^{\text{miss}}$); table 27 ($2L + (2-6)j + (E_T^{\text{miss}})$); table 28 ($3L + 4j + E_T^{\text{miss}}$); and table 29 ($4L + 4j$). The $\tilde{B}$ configurations apply to the other electroweakinos, and the colored LSPs.

JHEP07(2023)215

LSP	$\tilde{g}\tilde{g}$	$\tilde{g}\tilde{q}/\tilde{g}\bar{u}/\tilde{g}\bar{d}$	Squark Pair (1st,2nd gen.)	Squark Pair (3rd gen.)	$\tilde{W}\tilde{W}$	$\tilde{H}\tilde{H}$	Slepton Pair (1st, 2nd gen.)	Slepton Pair (3rd gen.)	$\tilde{B}\tilde{B}$
$\tilde{g}$	$+-$	$\times$	$\times$	$\times$	$\times$	$\times$	$\times$	$\times$	$\times$
$\tilde{q}/\tilde{u}/\tilde{d}$	$+2j_i$	$+j_i$	$+-$	$\times$	$\times$	$\times$	$\times$	$\times$	$\times$
$\tilde{q}_3/\tilde{t}/\tilde{b}$	$+2j_3$	$+j_i+2j_3$	$+2j_i+2j_3$	$+-$	$\times$	$\times$	$\times$	$\times$	$\times$
$\tilde{W}$	$+4j$	$+j_i+2j$	$+2j_i$	$+2j_3$	$+-$	$\times$	$\times$	$\times$	$\times$
$\tilde{H}$	$+4j$	$+j_i+2j$	$+2j_i$	$+2j_3$	$\times$	$+-$	$\times$	$\times$	$\times$
$\tilde{\ell}(\tilde{\nu})/\tilde{e}$	$\tilde{\ell}\tilde{\ell}/\tilde{\nu}\tilde{\nu}:\ +2\ell+4j$	$+2\ell+j_i+2j$	$+2\ell+2j_i$	$+2\ell+2j_3$	$+\ell+E_T^{\rm miss}$	$+2\ell$	$+-$	$\times$	$\times$
	$\tilde{\ell}\tilde{\nu}:\ +\ell+4j+E_T^{\rm miss}$	$+\ell+j_i+2j+E_T^{\rm miss}$	$+\ell+2j_i+E_T^{\rm miss}$	$+\ell+2j_3+E_T^{\rm miss}$	$+2\ell$	$+\ell+E_T^{\rm miss}$	$+-$	$\times$	$\times$
$\tilde{\tau}_L(\tilde{\nu}_\tau)/\tilde{\tau}_R$	$\tilde{\tau}_L\tilde{\tau}_L/\tilde{\tau}_R\tilde{\tau}_R:\ +2\tau+4j$	$+2\tau+j_i+2j$	$+2\tau+2j_i$	$+2\tau+2j_3$	$+\tau+E_T^{\rm miss}$	$+2\tau$	$+-$	$\times$	$\times$
	$\tilde{\tau}_L\tilde{\nu}_\tau:\ +\tau+4j+E_T^{\rm miss}$	$+\tau+j_i+2j+E_T^{\rm miss}$	$+\tau+2j_i+E_T^{\rm miss}$	$+\tau+2j_3+E_T^{\rm miss}$	$+2\tau$	$+\tau+E_T^{\rm miss}$	$+-$	$\times$	$\times$
$\tilde{B}$	$+4j$	$+j_i+2j$	$+2j_i$	$+2j_3$	$+3\ell+E_T^{\rm miss}/2\ell+E_T^{\rm miss}/4j/2v$	$+4j_3/2v$	$+2\ell/\ell+E_T^{\rm miss}$	$+2\tau/\tau+E_T^{\rm miss}$	$+-$

Table 17. Objects arising in the cascade decays of various pairs of parent sparticles (columns) down to the LSP(s) (rows). These can be added to the corresponding LSP signatures given in tables 2–11 to optimize searches. $+-$ indicates an empty set while $\times$ indicates that the corresponding production channel is not relevant for the given LSP because the cross-section is either lower than or comparable to the cross-section for direct pair production of the LSP.

JHEP07(2023)215

LSP	Coupling	Signature
$\tilde{e}_a$	$\lambda_{aba}\ a \neq b$	$\ell_a^+\ell_a^-/\ell_b^+\ell_b^-/\ell_a^+\ell_b^-$
$\tilde{e}_b$	λ_{a3b}	$\ell_a^+\ell_a^-/\ell_a^+\tau^-$
$\tilde{\tau}_R$	$\lambda_{ab3}\ a \neq b$	$\ell_a^+\ell_a^-/\ell_b^+\ell_b^-/\ell_a^+\ell_b^-$
$\tilde{\tau}_R$	λ_{a33}	$\ell_a^+\ell_a^-/\ell_a^+\tau^-$

Table 18. $2L + E_T^{\text{miss}}$.

LSP	Coupling	Signature
$\tilde{\ell}_a\,(\tilde{\nu}_a)$	$\lambda_{abc}\ a \neq b$	$\ell_b^+\ell_c^+\ell_c^-/\ell_b^-\ell_c^+\ell_c^+$
$\tilde{\ell}_a\,(\tilde{\nu}_a)$	λ_{a3b}	$\ell_b^+\ell_b^+\tau^-/\ell_b^+\ell_b^-\tau^+$
$\tilde{\ell}_a\,(\tilde{\nu}_a)$	$\lambda_{ab3}\ a \neq b$	$\ell_b^+\tau^+\tau^-/\ell_b^-\tau^+\tau^+$
$\tilde{\ell}_a\,(\tilde{\nu}_a)$	λ_{a33}	$\tau^+\tau^+\tau^-$
$\tilde{\tau}_L\,(\tilde{\nu}_\tau)$	λ_{a3b}	$\ell_a^-\ell_b^+\ell_b^+/\ell_a^+\ell_b^+\ell_b^-$
$\tilde{\tau}_L\,(\tilde{\nu}_\tau)$	λ_{a33}	$\ell_a^+\tau^+\tau^-/\ell_a^-\tau^+\tau^+$

Table 19. $3L + E_T^{\text{miss}}$.

LSP	Coupling	Signature
$\tilde{\ell}_a\,(\tilde{\nu}_a)$	$\lambda_{abc}\ a \neq b$	$\ell_b^+\ell_b^+\ell_c^-\ell_c^-/\ell_b^+\ell_b^-\ell_c^+\ell_c^-$
$\tilde{\ell}_a\,(\tilde{\nu}_a)$	λ_{a3b}	$\ell_b^-\ell_b^-\tau^+\tau^+/\ell_b^+\ell_b^-\tau^+\tau^-$
$\tilde{\ell}_a\,(\tilde{\nu}_a)$	$\lambda_{ab3}\ a \neq b$	$\ell_b^-\ell_b^-\tau^+\tau^+/\ell_b^+\ell_b^-\tau^+\tau^-$
$\tilde{\ell}_a\,(\tilde{\nu}_a)$	λ_{a33}	$\tau^+\tau^+\tau^-\tau^-$
$\tilde{\tau}_L\,(\tilde{\nu}_\tau)$	λ_{a3b}	$\ell_a^+\ell_a^+\ell_b^-\ell_b^-/\ell_a^+\ell_a^-\ell_b^+\ell_b^-$
$\tilde{\tau}_L\,(\tilde{\nu}_\tau)$	λ_{a33}	$\ell_a^-\ell_a^-\tau^+\tau^+/\ell_a^+\ell_a^-\tau^+\tau^-$

Table 20. $4L$.

LSP	Coupling	Signature
$\tilde{B}$	$\lambda_{ijk}\ i \neq j$	$\ell_i^+\ell_i^+\ell_k^-\ell_k^-/\ell_i^+\ell_i^-\ell_k^+\ell_k^-/\ell_j^+\ell_j^+\ell_k^-\ell_k^-/\ell_j^+\ell_j^-\ell_k^+\ell_k^-/\ell_i^+\ell_j^+\ell_k^-\ell_k^-/\ell_i^+\ell_j^-\ell_k^+\ell_k^-$
$\tilde{W}$	$\lambda_{ijk}\ i \neq j$	$\ell_i^+\ell_j^+\ell_k^-\ell_k^-/\ell_i^+\ell_j^-\ell_k^+\ell_k^-$

Table 21. $4L + (0-4)j + E_T^{\text{miss}}$.

LSP	Coupling	Signature
$\tilde{\tau}_L\,(\tilde{\nu})$	$\lambda_{aba}\ a \neq b$	$\ell_a^+\ell_a^+\ell_a^-\ell_a^-\tau^+/\ell_a^+\ell_a^-\ell_b^+\ell_b^-\tau^+/\ell_a^+\ell_a^+\ell_b^-\ell_b^-\tau^+/\ell_a^+\ell_a^+\ell_a^-\ell_b^+\tau^+$
$\tilde{\tau}_L\,(\tilde{\nu})$	$\lambda_{ab3}\ a \neq b$	$\ell_a^-\ell_a^-\tau^+\tau^+\tau^+/\ell_b^-\ell_b^-\tau^+\tau^+\tau^+/\ell_a^+\ell_a^-\tau^+\tau^+\tau^-/\ell_b^+\ell_b^-\tau^+\tau^+\tau^-/\ell_a^-\ell_b^-\tau^+\tau^+\tau^+/\ell_a^+\ell_b^-\tau^+\tau^+\tau^-$

Table 22. $5L + E_T^{\text{miss}}$.

LSP	Coupling	Signature
$\tilde{e}_a$	$\lambda_{ab3}\ a \neq b$	$\ell_a^+\ell_a^-\ell_a^-\tau^+\tau^+/\ell_a^+\ell_a^-\ell_b^-\ell_b^-\tau^+\tau^+/\ell_a^+\ell_a^+\ell_a^-\ell_b^-\tau^+\tau^-/\ell_a^+\ell_a^-\ell_a^-\ell_b^+\ell_b^-\tau^+\tau^-/\ell_a^+\ell_a^-\ell_a^-\ell_b^-\tau^+\tau^+/\ell_a^+\ell_a^+\ell_a^-\ell_b^-\tau^+\tau^-$
$\tilde{e}_b$	λ_{a33}	$\ell_a^+\ell_a^-\ell_a^-\tau^+\tau^+\tau^-/\ell_a^+\ell_a^-\ell_a^-\ell_a^-\tau^+\tau^+/\ell_a^+\ell_a^+\ell_a^-\ell_a^-\tau^+\tau^-$
$\tilde{\tau}_L\,(\tilde{\nu})$	$\lambda_{aba}\ a \neq b$	$\ell_a^+\ell_a^+\ell_a^-\ell_a^-\tau^+\tau^-/\ell_a^+\ell_a^-\ell_b^+\ell_b^-\tau^+\tau^-/\ell_a^+\ell_a^+\ell_b^-\ell_b^-\tau^+\tau^-/\ell_a^+\ell_a^+\ell_a^-\ell_b^+\tau^+\tau^-$
$\tilde{\tau}_L\,(\tilde{\nu})$	$\lambda_{ab3}\ a \neq b$	$\ell_a^-\ell_a^-\tau^+\tau^+\tau^+\tau^-/\ell_b^-\ell_b^-\tau^+\tau^+\tau^+\tau^-/\ell_a^+\ell_a^-\tau^+\tau^+\tau^-\tau^-/\ell_b^+\ell_b^-\tau^+\tau^+\tau^-\tau^-/\ell_a^-\ell_b^-\tau^+\tau^+\tau^+\tau^-/\ell_a^+\ell_b^-\tau^+\tau^+\tau^-\tau^-$
$\tilde{\tau}_R$	$\lambda_{aba}\ a \neq b$	$\ell_a^+\ell_a^+\ell_a^-\ell_a^-\tau^+\tau^-/\ell_a^+\ell_a^-\ell_b^+\ell_b^-\tau^+\tau^-/\ell_a^+\ell_a^+\ell_b^-\ell_b^-\tau^+\tau^-/\ell_a^+\ell_a^-\ell_a^-\ell_b^+\tau^+\tau^-$
$\tilde{\tau}_R$	λ_{a3b}	$\ell_a^+\ell_a^+\ell_b^-\ell_b^-\tau^+\tau^-/\ell_a^+\ell_a^-\ell_b^+\ell_b^-\tau^+\tau^-/\ell_a^+\ell_a^-\ell_b^-\ell_b^-\tau^+\tau^+\tau^-/\ell_a^-\ell_b^+\ell_b^-\tau^+\tau^+\tau^-$

Table 23. $6L + E_T^{\text{miss}}$.

LSP	Coupling	Signature
$\tilde{\ell}_a\,(\tilde{\nu}_a)$	λ''_{ijk}	ℓ_a^+
$\tilde{\tau}_L\,(\tilde{\nu})$	λ''_{ijk}	τ^+

Table 24. $1L + 2j_l + 4j + E_T^{\text{miss}}$.

LSP	Coupling	Signature
$\tilde{\ell}_a\,(\tilde{\nu}_a)$	λ''_{ijk}	$\ell_a^+\ell_a^-$
$\tilde{e}_a$	λ''_{ijk}	$\ell_a^+\ell_a^-$
$\tilde{\tau}_L\,(\tilde{\nu})$	λ''_{ijk}	$\tau^+\tau^-$
$\tilde{\tau}_R$	λ''_{ijk}	$\tau^+\tau^-$

Table 25. $2L + 2j_l + 4j$.

JHEP07(2023)215

LSP	Coupling	Signature
$\tilde{B}$	λ'_{ijk}	ℓ_i^+
$\tilde{\ell}_a(\tilde{\nu}_a)$	λ'_{33k}	ℓ_a^+
$\tilde{\tau}_L\,(\tilde{\nu}_\tau)$	λ'_{a3k}	τ^+

Table 26. $1L + (2-6)j + E_T^{\rm miss}$.

LSP	Coupling	Signature
$\tilde{B}$	λ'_{ijk}	$\ell_i^+\ell_i^-/\ell_i^+\ell_i^+$
$\tilde{\ell}_a(\tilde{\nu}_a)$	λ'_{3ak}	$\ell_a^+\tau^+/\ell_a^+\tau^-$
$\tilde{\ell}_a(\tilde{\nu}_a)$	λ'_{33k}	$\ell_a^+\ell_a^-/\ell_a^+\tau^+/\ell_a^+\tau^-$
$\tilde{\tau}_L\,(\tilde{\nu}_\tau)$	λ'_{abk}	$\ell_a^+\tau^+/\ell_a^+\tau^-$
$\tilde{\tau}_L\,(\tilde{\nu}_\tau)$	λ'_{a3k}	$\ell_a^+\tau^+/\ell_a^+\tau^-/\tau^+\tau^-$
$\tilde{e}_a$	λ'_{i3k}	$\ell_a^+\ell_a^-$
$\tilde{\tau}$	λ'_{i3k}	$\tau^+\tau^-$

Table 27. $2L + (2-6)j + (E_T^{\rm miss})$.

LSP	Coupling	Signature
$\tilde{\ell}_a(\tilde{\nu}_a)$	λ'_{3jk}	$\ell_a^+\ell_a^-\tau^+/\ell_a^+\tau^+\tau^-/\ell_a^+\tau^+\tau^+/\ell_a^+\tau^-\tau^-$
$\tilde{\tau}_L\,(\tilde{\nu}_\tau)$	λ'_{ajk}	$\ell_a^+\ell_a^-\tau^+/\ell_a^+\ell_a^+\tau^+/\ell_a^-\ell_a^-\tau^+/\ell_a^+\tau^+\tau^-$
$\tilde{e}_a$	λ'_{ijk}	$\ell_a^+\ell_a^-\ell_i^+$
$\tilde{\tau}$	λ'_{i3k}	$\ell_i^+\tau^+\tau^-$

Table 28. $3L + 4j + E_T^{\rm miss}$.

LSP	Coupling	Signature
$\tilde{\ell}_a(\tilde{\nu}_a)$	λ'_{3jk}	$\ell_a^+\ell_a^-\tau^+\tau^-/\ell_a^+\ell_a^-\tau^+\tau^+$
$\tilde{\tau}_L\,(\tilde{\nu}_\tau)$	λ'_{ajk}	$\ell_a^+\ell_a^-\tau^+\tau^-/\ell_a^+\ell_a^+\tau^+\tau^-$
$\tilde{e}_a$	λ'_{ijk}	$\ell_a^+\ell_a^-\ell_i^+\ell_i^-/\ell_a^+\ell_a^-\ell_i^+\ell_i^+$
$\tilde{\tau}$	λ'_{i3k}	$\ell_i^+\ell_i^-\tau^+\tau^-/\ell_i^+\ell_i^+\tau^+\tau^-$

Table 29. $4L + 4j$.

C `abc-rpv`, the RPV Python library

`abc-rpv`[15] is a Python library that provides a framework for analyzing the collider signatures of the RPV-MSSM. Users are provided with various functionalities to explore the landscape of RPV-MSSM physics within the context of small RPV couplings. In this section, we provide a short introduction to the library. A complete manual will be provided as a separate document/paper in the future.

C.1 Introduction

The code starts by generating all possible transitions from one sparticle to another, based on the vertices provided in the input table (`table_notsup.csv`) stored in the input directory. Using this, it can obtain the resulting signature for a decay chain from any LSP to a sparticle directly coupled to an RPV operator; the latter, then, simply decays into purely Standard Model objects. Going through all combinations of LSP type, and RPV couplings (in terms of categories defined in tables 2–11), all possible decay chains and signatures are compiled into tables. These tables are the output available to the user that can then be analyzed using the functions described below. By default, all output tables are already

[15] `abc-rpv` Python library is available at: https://github.com/kys-sheng/abc-rpv.git.

JHEP07(2023)215

generated using the default input table, and are readily available in the data directory. The user does not need to generate the tables unless the input table is modified.

C.2 Assumptions and caveats

In the implementation of our code, there are a few assumptions and caveats worth noting:

- All possible transitions are constructed from vertices provided in `table_notsup.csv` in the input directory. The vertices provided in this table need not be a 3-point vertex.
- The input table (`table_notsup.csv`) contains vertices that allow transitions from one sparticle to another while producing standard model particles. By default, only non-suppressed transitions based on the MSSM interactions are included; we use modified versions of the tables compiled in ref. [96] for classifying vertices as suppressed or non-suppressed. Note that the input table can be modified by the user, as needed. This allows one to regenerate the output tables with custom vertices.
- While generating the decay chains for the LSPs, only the shortest chain is constructed by default. Users also have the option to generate all possible chains up to 3 transitions.
- The decay chains do not contain repeating sparticles.

C.3 Usage

Please refer to `Tutorial.ipynb` available at https://github.com/kys-sheng/abc-rpv.git for a complete tutorial of the Python library. We only discuss basic functionality here.

Syntax. Tables 30 and 31 show the syntax used in the code. One can also refer to `rpv_definitions.py` for more information.

Dictionaries. In the library, there are a few built-in dictionaries that contain the output tables generated from the code.

- `ONE_LSP_RPV_DECAY_DICT`: contains details for all possible RPV decays of one LSP. Information regarding RPV coupling category, signature, decay chains, number of vertices is included.
- `TWO_LSP_RPV_DECAY_DICT`: contains details for all possible RPV decays of a pair[16] of LSPs (decay via same category of RPV coupling). Information regarding RPV coupling category, signature, decay chains, number of vertices is included.
- `TWO_LSP_MIXED_RPV_DECAY_DICT`: contains details for all possible RPV decays of a pair of LSPs (decay via different categories of RPV couplings). Information regarding RPV coupling categories, signature, decay chains, number of vertices is included.
- `ONE_LSP_SIG_CAT_DICT`: contains final state signatures arising from decay of one LSP, categorized by RPV coupling; similar to tables 2–11.

[16] We restrict to the case where both LSPs are the same, or belong to the same $SU(2)_L$ doublet.

JHEP07(2023)215

Code Syntax	Sparticles
B	Bino, B
W^+	Charged Wino
W^0	Neutral Wino
G	Gluino
H^+	Charged Higgsino
H^0	Neutral Higgsino
q	$\tilde{u}_L$, $\tilde{d}_L$, $\tilde{c}_L$, $\tilde{s}_L$
d	$\tilde{d}_R$, $\tilde{s}_R$
u	$\tilde{u}_R$, $\tilde{c}_R$
l	$\tilde{e}_L$, $\tilde{\mu}_L$
nu	$\tilde{\nu}_e$, $\tilde{\nu}_\mu$
e	$\tilde{e}_R$, $\tilde{\mu}_R$
t_L	$\tilde{t}_L$
b_L	$\tilde{b}_L$
t	$\tilde{t}_R$
b	$\tilde{b}_R$
tau_L	$\tilde{\tau}_L$
tau	$\tilde{\tau}_R$
nu_tau	$\tilde{\nu}_\tau$

Table 30. Syntax for sparticles used in the code.

Symbol	Particles (Final State Objects)
l	e/μ
T	τ
L	$e/\mu/\tau$
j	$u/d/c/s$ jets
b	b jets
t	t jets
3	t/b jets
J	$u/d/c/s/t/b$ jets
v	$W/Z/h$
X	MET

Table 31. One-character syntax for final state objects used in the code.

JHEP07(2023)215

- `TWO_LSP_SIG_CAT_DICT`: contains final state signatures arising from decay of pair of LSPs, categorized by RPV coupling; similar to tables 2–11.

Note that the above dictionaries are regenerated upon using different input transition tables, as well as different table generation choices (e.g., decay chain length).

Main functions. Although the dictionaries by themselves contain all relevant information, it is more efficient and powerful to use the functions provided in the library to analyze the data. We describe the basic usage here; refer to `Tutorial.ipynb` for more details.

One LSP decay.

- `find_one_lsp_from_signature`
  Using the signature as input, this function finds all LSPs with decay chains leading to the given final state. Alongside with the LSP, the relevant RPV couplings and decay chains are also returned.

- `find_one_lsp_from_signature_inclusive`
  Similar to `find_one_lsp_from_signature`, but in the inclusive mode (e.g., one can choose $n_{jets} > 3$ instead of $n_{jets} = 3$).

- `find_signatures_from_one_lsp`
  Using the LSP as input, this function finds all possible signatures that can arise in the LSP decay. Alongside with the signatures, the relevant RPV couplings and decay chains are also returned.

LSP pair decay; same coupling category.

- `find_two_lsp_from_signature`:
  Similar to `find_one_lsp_from_signature` but returns all pairs of LSPs leading to the input signature.

- `find_two_lsp_from_signature_inclusive`:
  Inclusive mode of `find_two_lsp_from_signature`.

- `find_signatures_from_two_lsp`:
  Similar to `find_signatures_from_one_lsp` but for a pair of input LSPs.

In all of the above, the pair is assumed to decay via the same (category of) RPV coupling.

LSP pair decay; different coupling categories.

- `find_two_lsp_from_signature_mixed_couplings`

- `find_two_lsp_from_signature_mixed_couplings_inclusive`

- `find_signatures_from_two_lsp_mixed_couplings`

Analogous to the above but for LSP pair decaying via different (categories of) RPV couplings.

JHEP07(2023)215

Advanced usage. By default, all dictionaries and tables are regenerated automatically from the input table if all the csv files in the data directory are deleted. Thus, users can generate all the tables based on their custom input table (`table_notsup.csv`) by deleting the csv files in the data directory and reimporting the library. A step-by-step example demonstrating this will be provided in the complete manual.

References

[1] Y.A. Golfand and E.P. Likhtman, *Extension of the algebra of Poincare group generators and violation of p invariance*, *JETP Lett.* **13** (1971) 323 [INSPIRE].

[2] D.V. Volkov and V.P. Akulov, *Is the neutrino a Goldstone particle?*, *Phys. Lett. B* **46** (1973) 109 [INSPIRE].

[3] J. Wess and B. Zumino, *A Lagrangian model invariant under supergauge transformations*, *Phys. Lett. B* **49** (1974) 52 [INSPIRE].

[4] J. Wess and B. Zumino, *Supergauge transformations in four-dimensions*, *Nucl. Phys. B* **70** (1974) 39 [INSPIRE].

[5] S.R. Coleman and J. Mandula, *All possible symmetries of the S matrix*, *Phys. Rev.* **159** (1967) 1251 [INSPIRE].

[6] R. Haag, J.T. Lopuszanski and M. Sohnius, *All possible generators of supersymmetries of the S matrix*, *Nucl. Phys. B* **88** (1975) 257 [INSPIRE].

[7] E. Gildener, *Gauge symmetry hierarchies*, *Phys. Rev. D* **14** (1976) 1667 [INSPIRE].

[8] M.J.G. Veltman, *The infrared-ultraviolet connection*, *Acta Phys. Polon. B* **12** (1981) 437 [INSPIRE].

[9] H.P. Nilles, *Supersymmetry, supergravity and particle physics*, *Phys. Rept.* **110** (1984) 1 [INSPIRE].

[10] S.P. Martin, *A supersymmetry primer*, *Adv. Ser. Direct. High Energy Phys.* **18** (1998) 1 [hep-ph/9709356] [INSPIRE].

[11] M. Drees, R. Godbole and P. Roy, *Theory and phenomenology of sparticles: an account of four-dimensional $N = 1$ supersymmetry in high energy physics*, (2004) [INSPIRE].

[12] ATLAS collaboration, *SUSY March 2023 summary plot update*, ATL-PHYS-PUB-2023-005, CERN, Geneva, Switzerland (2023).

[13] ATLAS collaboration, *Search for supersymmetry in final states with missing transverse momentum and three or more b-jets in 139 fb^{-1} of proton-proton collisions at $\sqrt{s} = 13$ TeV with the ATLAS detector*, *Eur. Phys. J. C* **83** (2023) 561 [arXiv:2211.08028] [INSPIRE].

[14] ATLAS collaboration, *Search for new phenomena in final states with photons, jets and missing transverse momentum in pp collisions at $\sqrt{s} = 13$ TeV with the ATLAS detector*, *JHEP* **07** (2023) 021 [arXiv:2206.06012] [INSPIRE].

[15] ATLAS collaboration, *Search for new phenomena in pp collisions in final states with tau leptons, b-jets, and missing transverse momentum with the ATLAS detector*, *Phys. Rev. D* **104** (2021) 112005 [arXiv:2108.07665] [INSPIRE].

JHEP07(2023)215

[16] ATLAS collaboration, *Search for new phenomena in events with two opposite-charge leptons, jets and missing transverse momentum in pp collisions at $\sqrt{s} = 13$ TeV with the ATLAS detector*, *JHEP* **04** (2021) 165 [arXiv:2102.01444] [INSPIRE].

[17] ATLAS collaboration, *Search for new phenomena in final states with b-jets and missing transverse momentum in $\sqrt{s} = 13$ TeV pp collisions with the ATLAS detector*, *JHEP* **05** (2021) 093 [arXiv:2101.12527] [INSPIRE].

[18] ATLAS collaboration, *Search for squarks and gluinos in final states with one isolated lepton, jets, and missing transverse momentum at $\sqrt{s} = 13$ TeV with the ATLAS detector*, *Eur. Phys. J. C* **81** (2021) 600 [*Erratum ibid.* **81** (2021) 956] [arXiv:2101.01629] [INSPIRE].

[19] ATLAS collaboration, *Search for new phenomena with top quark pairs in final states with one lepton, jets, and missing transverse momentum in pp collisions at $\sqrt{s} = 13$ TeV with the ATLAS detector*, *JHEP* **04** (2021) 174 [arXiv:2012.03799] [INSPIRE].

[20] ATLAS collaboration, *Search for squarks and gluinos in final states with jets and missing transverse momentum using 139 fb^{-1} of $\sqrt{s} = 13$ TeV pp collision data with the ATLAS detector*, *JHEP* **02** (2021) 143 [arXiv:2010.14293] [INSPIRE].

[21] ATLAS collaboration, *Search for new phenomena in final states with large jet multiplicities and missing transverse momentum using $\sqrt{s} = 13$ TeV proton-proton collisions recorded by ATLAS in run 2 of the LHC*, *JHEP* **10** (2020) 062 [arXiv:2008.06032] [INSPIRE].

[22] ATLAS collaboration, *Search for a scalar partner of the top quark in the all-hadronic $t\bar{t}$ plus missing transverse momentum final state at $\sqrt{s} = 13$ TeV with the ATLAS detector*, *Eur. Phys. J. C* **80** (2020) 737 [arXiv:2004.14060] [INSPIRE].

[23] ATLAS collaboration, *Search for squarks and gluinos in final states with same-sign leptons and jets using 139 fb^{-1} of data collected with the ATLAS detector*, *JHEP* **06** (2020) 046 [arXiv:1909.08457] [INSPIRE].

[24] ATLAS collaboration, *Search for bottom-squark pair production with the ATLAS detector in final states containing Higgs bosons, b-jets and missing transverse momentum*, *JHEP* **12** (2019) 060 [arXiv:1908.03122] [INSPIRE].

[25] CMS collaboration, *Search for higgsinos decaying to two Higgs bosons and missing transverse momentum in proton-proton collisions at $\sqrt{s} = 13$ TeV*, *JHEP* **05** (2022) 014 [arXiv:2201.04206] [INSPIRE].

[26] CMS collaboration, *Combined searches for the production of supersymmetric top quark partners in proton-proton collisions at $\sqrt{s} = 13$ TeV*, *Eur. Phys. J. C* **81** (2021) 970 [arXiv:2107.10892] [INSPIRE].

[27] CMS collaboration, *Search for supersymmetry in final states with two or three soft leptons and missing transverse momentum in proton-proton collisions at $\sqrt{s} = 13$ TeV*, *JHEP* **04** (2022) 091 [arXiv:2111.06296] [INSPIRE].

[28] CMS collaboration, *Search for supersymmetry in final states with two oppositely charged same-flavor leptons and missing transverse momentum in proton-proton collisions at $\sqrt{s} = 13$ TeV*, *JHEP* **04** (2021) 123 [arXiv:2012.08600] [INSPIRE].

[29] CMS collaboration, *Search for physics beyond the standard model in events with jets and two same-sign or at least three charged leptons in proton-proton collisions at $\sqrt{s} = 13$ TeV*, *Eur. Phys. J. C* **80** (2020) 752 [arXiv:2001.10086] [INSPIRE].

JHEP07(2023)215

[30] CMS collaboration, *Search for supersymmetry in proton-proton collisions at $\sqrt{s} = 13$ TeV in events with high-momentum Z bosons and missing transverse momentum*, *JHEP* **09** (2020) 149 [arXiv:2008.04422] [INSPIRE].

[31] CMS collaboration, *Search for supersymmetry in pp collisions at $\sqrt{s} = 13$ TeV with 137 fb^{-1} in final states with a single lepton using the sum of masses of large-radius jets*, *Phys. Rev. D* **101** (2020) 052010 [arXiv:1911.07558] [INSPIRE].

[32] CMS collaboration, *Search for top squark pair production in a final state with two tau leptons in proton-proton collisions at $\sqrt{s} = 13$ TeV*, *JHEP* **02** (2020) 015 [arXiv:1910.12932] [INSPIRE].

[33] CMS collaboration, *Searches for physics beyond the standard model with the M_{T2} variable in hadronic final states with and without disappearing tracks in proton-proton collisions at $\sqrt{s} = 13$ TeV*, *Eur. Phys. J. C* **80** (2020) 3 [arXiv:1909.03460] [INSPIRE].

[34] CMS collaboration, *Search for supersymmetry in proton-proton collisions at 13 TeV in final states with jets and missing transverse momentum*, *JHEP* **10** (2019) 244 [arXiv:1908.04722] [INSPIRE].

[35] CMS collaboration, *Search for supersymmetry in final states with a single electron or muon using angular correlations and heavy-object identification in proton-proton collisions at $\sqrt{s} = 13$ TeV*, arXiv:2211.08476 [INSPIRE].

[36] ATLAS collaboration, *Search for direct pair production of sleptons and charginos decaying to two leptons and neutralinos with mass splittings near the W-boson mass in $\sqrt{s} = 13$ TeV pp collisions with the ATLAS detector*, *JHEP* **06** (2023) 031 [arXiv:2209.13935] [INSPIRE].

[37] ATLAS collaboration, *Search for charginos and neutralinos in final states with two boosted hadronically decaying bosons and missing transverse momentum in pp collisions at $\sqrt{s} = 13$ TeV with the ATLAS detector*, *Phys. Rev. D* **104** (2021) 112010 [arXiv:2108.07586] [INSPIRE].

[38] ATLAS collaboration, *Search for chargino-neutralino pair production in final states with three leptons and missing transverse momentum in $\sqrt{s} = 13$ TeV pp collisions with the ATLAS detector*, *Eur. Phys. J. C* **81** (2021) 1118 [arXiv:2106.01676] [INSPIRE].

[39] ATLAS collaboration, *Search for chargino-neutralino production with mass splittings near the electroweak scale in three-lepton final states in $\sqrt{s} = 13$ TeV pp collisions with the ATLAS detector*, *Phys. Rev. D* **101** (2020) 072001 [arXiv:1912.08479] [INSPIRE].

[40] ATLAS collaboration, *Searches for electroweak production of supersymmetric particles with compressed mass spectra in $\sqrt{s} = 13$ TeV pp collisions with the ATLAS detector*, *Phys. Rev. D* **101** (2020) 052005 [arXiv:1911.12606] [INSPIRE].

[41] ATLAS collaboration, *Search for direct stau production in events with two hadronic τ-leptons in $\sqrt{s} = 13$ TeV pp collisions with the ATLAS detector*, *Phys. Rev. D* **101** (2020) 032009 [arXiv:1911.06660] [INSPIRE].

[42] ATLAS collaboration, *Search for direct production of electroweakinos in final states with one lepton, missing transverse momentum and a Higgs boson decaying into two b-jets in pp collisions at $\sqrt{s} = 13$ TeV with the ATLAS detector*, *Eur. Phys. J. C* **80** (2020) 691 [arXiv:1909.09226] [INSPIRE].

[43] CMS collaboration, *Search for electroweak production of charginos and neutralinos in proton-proton collisions at $\sqrt{s} = 13$ TeV*, *JHEP* **04** (2022) 147 [arXiv:2106.14246] [INSPIRE].

JHEP07(2023)215

[44] CMS collaboration, *Search for electroweak production of charginos and neutralinos in multilepton final states in proton-proton collisions at* $\sqrt{s} = 13$ *TeV*, *JHEP* **03** (2018) 166 [arXiv:1709.05406] [INSPIRE].

[45] CMS collaboration, *Search for chargino-neutralino production in events with Higgs and W bosons using* $137\,fb^{-1}$ *of proton-proton collisions at* $\sqrt{s} = 13$ *TeV*, *JHEP* **10** (2021) 045 [arXiv:2107.12553] [INSPIRE].

[46] CMS collaboration, *Search for supersymmetric partners of electrons and muons in proton-proton collisions at* $\sqrt{s} = 13$ *TeV*, *Phys. Lett. B* **790** (2019) 140 [arXiv:1806.05264] [INSPIRE].

[47] CMS collaboration, *Search for direct pair production of supersymmetric partners of* τ *leptons in the final state with two hadronically decaying* τ *leptons and missing transverse momentum in proton-proton collisions at* $\sqrt{s} = 13$ *TeV*, arXiv:2207.02254 [INSPIRE].

[48] CMS collaboration, *Search for supersymmetry with a compressed mass spectrum in events with a soft* τ *lepton, a highly energetic jet, and large missing transverse momentum in proton-proton collisions at* $\sqrt{s} = 13$ *TeV*, *Phys. Rev. Lett.* **124** (2020) 041803 [arXiv:1910.01185] [INSPIRE].

[49] CMS collaboration, *Search for supersymmetry using Higgs boson to diphoton decays at* $\sqrt{s} = 13$ *TeV*, *JHEP* **11** (2019) 109 [arXiv:1908.08500] [INSPIRE].

[50] CMS collaboration, *Search for electroweak production of charginos and neutralinos at* $\sqrt{s} = 13$ *TeV in final states containing hadronic decays of* WW, WZ, *or* WH *and missing transverse momentum*, *Phys. Lett. B* **842** (2023) 137460 [arXiv:2205.09597] [INSPIRE].

[51] CMS collaboration, *Search for direct pair production of supersymmetric partners to the* τ *lepton in proton-proton collisions at* $\sqrt{s} = 13$ *TeV*, *Eur. Phys. J. C* **80** (2020) 189 [arXiv:1907.13179] [INSPIRE].

[52] P. Bechtle et al., *What if the LHC does not find supersymmetry in the* $\sqrt{s} = 7$ *TeV run?*, *Phys. Rev. D* **84** (2011) 011701 [arXiv:1102.4693] [INSPIRE].

[53] J.A. Evans, Y. Kats, D. Shih and M.J. Strassler, *Toward full LHC coverage of natural supersymmetry*, *JHEP* **07** (2014) 101 [arXiv:1310.5758] [INSPIRE].

[54] M. Lisanti, P. Schuster, M. Strassler and N. Toro, *Study of LHC searches for a lepton and many jets*, *JHEP* **11** (2012) 081 [arXiv:1107.5055] [INSPIRE].

[55] ATLAS collaboration, *Search for R-parity-violating supersymmetry in a final state containing leptons and many jets with the ATLAS experiment using* $\sqrt{s} = 13$ *TeV proton-proton collision data*, *Eur. Phys. J. C* **81** (2021) 1023 [arXiv:2106.09609] [INSPIRE].

[56] CMS collaboration, *Search for top squarks in final states with two top quarks and several light-flavor jets in proton-proton collisions at* $\sqrt{s} = 13$ *TeV*, *Phys. Rev. D* **104** (2021) 032006 [arXiv:2102.06976] [INSPIRE].

[57] S. Weinberg, *Supersymmetry at ordinary energies. 1. Masses and conservation laws*, *Phys. Rev. D* **26** (1982) 287 [INSPIRE].

[58] H.K. Dreiner, *An introduction to explicit R-parity violation*, *Adv. Ser. Direct. High Energy Phys.* **21** (2010) 565 [hep-ph/9707435] [INSPIRE].

[59] R. Barbier et al., *R-parity violating supersymmetry*, *Phys. Rept.* **420** (2005) 1 [hep-ph/0406039] [INSPIRE].

JHEP07(2023)215

[60] G.R. Farrar and P. Fayet, *Phenomenology of the production, decay, and detection of new hadronic states associated with supersymmetry*, *Phys. Lett. B* **76** (1978) 575 [INSPIRE].

[61] N. Chamoun, F. Domingo and H.K. Dreiner, *Nucleon decay in the R-parity violating MSSM*, *Phys. Rev. D* **104** (2021) 015020 [arXiv:2012.11623] [INSPIRE].

[62] PARTICLE DATA GROUP collaboration, *Review of particle physics*, *PTEP* **2022** (2022) 083C01 [INSPIRE].

[63] L.E. Ibanez and G.G. Ross, *Discrete gauge symmetries and the origin of baryon and lepton number conservation in supersymmetric versions of the standard model*, *Nucl. Phys. B* **368** (1992) 3 [INSPIRE].

[64] L.E. Ibanez and G.G. Ross, *Discrete gauge symmetry anomalies*, *Phys. Lett. B* **260** (1991) 291 [INSPIRE].

[65] H.K. Dreiner, M. Hanussek and C. Luhn, *What is the discrete gauge symmetry of the R-parity violating MSSM?*, *Phys. Rev. D* **86** (2012) 055012 [arXiv:1206.6305] [INSPIRE].

[66] H.K. Dreiner, M. Kramer and J. Tattersall, *How low can SUSY go? Matching, monojets and compressed spectra*, *EPL* **99** (2012) 61001 [arXiv:1207.1613] [INSPIRE].

[67] B.C. Allanach, A. Dedes and H.K. Dreiner, *R parity violating minimal supergravity model*, *Phys. Rev. D* **69** (2004) 115002 [*Erratum ibid.* **72** (2005) 079902] [hep-ph/0309196] [INSPIRE].

[68] F. de Campos et al., *Probing bilinear R-parity violating supergravity at the LHC*, *JHEP* **05** (2008) 048 [arXiv:0712.2156] [INSPIRE].

[69] L.J. Hall and M. Suzuki, *Explicit R-parity breaking in supersymmetric models*, *Nucl. Phys. B* **231** (1984) 419 [INSPIRE].

[70] H.K. Dreiner and M. Thormeier, *Supersymmetric Froggatt-Nielsen models with baryon and lepton number violation*, *Phys. Rev. D* **69** (2004) 053002 [hep-ph/0305270] [INSPIRE].

[71] L. Lee, C. Ohm, A. Soffer and T.-T. Yu, *Collider searches for long-lived particles beyond the Standard Model*, *Prog. Part. Nucl. Phys.* **106** (2019) 210 [*Erratum ibid.* **122** (2022) 103912] [arXiv:1810.12602] [INSPIRE].

[72] J. Alimena et al., *Searching for long-lived particles beyond the Standard Model at the Large Hadron Collider*, *J. Phys. G* **47** (2020) 090501 [arXiv:1903.04497] [INSPIRE].

[73] D. Acosta et al., *Review of opportunities for new long-lived particle triggers in run 3 of the Large Hadron Collider*, arXiv:2110.14675 [INSPIRE].

[74] ATLAS collaboration, *Search for long-lived, massive particles in events with displaced vertices and multiple jets in pp collisions at $\sqrt{s} = 13$ TeV with the ATLAS detector*, *JHEP* **2306** (2023) 200 [arXiv:2301.13866] [INSPIRE].

[75] ATLAS collaboration, *Search for displaced leptons in $\sqrt{s} = 13$ TeV pp collisions with the ATLAS detector*, *Phys. Rev. Lett.* **127** (2021) 051802 [arXiv:2011.07812] [INSPIRE].

[76] ATLAS collaboration, *Search for long-lived, massive particles in events with a displaced vertex and a muon with large impact parameter in pp collisions at $\sqrt{s} = 13$ TeV with the ATLAS detector*, *Phys. Rev. D* **102** (2020) 032006 [arXiv:2003.11956] [INSPIRE].

[77] CMS collaboration, *Search for long-lived particles using displaced jets in proton-proton collisions at $\sqrt{s} = 13$ TeV*, *Phys. Rev. D* **104** (2021) 012015 [arXiv:2012.01581] [INSPIRE].

[78] CMS collaboration, *Search for long-lived particles decaying to leptons with large impact parameter in proton-proton collisions at $\sqrt{s} = 13$ TeV*, *Eur. Phys. J. C* **82** (2022) 153 [arXiv:2110.04809] [INSPIRE].

JHEP07(2023)215

[79] CMS collaboration, *Search for long-lived particles decaying into muon pairs in proton-proton collisions at $\sqrt{s} = 13$ TeV collected with a dedicated high-rate data stream*, *JHEP* **04** (2022) 062 [arXiv:2112.13769] [INSPIRE].

[80] CMS collaboration, *Search for long-lived particles decaying to a pair of muons in proton-proton collisions at $\sqrt{s} = 13$ TeV*, *JHEP* **05** (2023) 228 [arXiv:2205.08582] [INSPIRE].

[81] CMS collaboration, *Search for long-lived particles using out-of-time trackless jets in proton-proton collisions at $\sqrt{s} = 13$ TeV*, arXiv:2212.06695 [INSPIRE].

[82] CMS collaboration, *Search for long-lived particles decaying to jets with displaced vertices in proton-proton collisions at $\sqrt{s} = 13$ TeV*, *Phys. Rev. D* **104** (2021) 052011 [arXiv:2104.13474] [INSPIRE].

[83] S. Dimopoulos, R. Esmailzadeh, L.J. Hall and G.D. Starkman, *Cross-sections for lepton and baryon number violating processes from supersymmetry at $p\bar{p}$ colliders*, *Phys. Rev. D* **41** (1990) 2099 [INSPIRE].

[84] H.K. Dreiner and G.G. Ross, *R-parity violation at hadron colliders*, *Nucl. Phys. B* **365** (1991) 597 [INSPIRE].

[85] H.K. Dreiner, P. Richardson and M.H. Seymour, *Resonant slepton production in hadron hadron collisions*, *Phys. Rev. D* **63** (2001) 055008 [hep-ph/0007228] [INSPIRE].

[86] H.K. Dreiner and T. Stefaniak, *Bounds on R-parity violation from resonant slepton production at the LHC*, *Phys. Rev. D* **86** (2012) 055010 [arXiv:1201.5014] [INSPIRE].

[87] A. Monteux, *New signatures and limits on R-parity violation from resonant squark production*, *JHEP* **03** (2016) 216 [arXiv:1601.03737] [INSPIRE].

[88] H.K. Dreiner, C. Hanhart, U. Langenfeld and D.R. Phillips, *Supernovae and light neutralinos: SN1987A bounds on supersymmetry revisited*, *Phys. Rev. D* **68** (2003) 055004 [hep-ph/0304289] [INSPIRE].

[89] H.K. Dreiner et al., *Mass bounds on a very light neutralino*, *Eur. Phys. J. C* **62** (2009) 547 [arXiv:0901.3485] [INSPIRE].

[90] J. de Vries, H.K. Dreiner and D. Schmeier, *R-parity violation and light neutralinos at SHiP and the LHC*, *Phys. Rev. D* **94** (2016) 035006 [arXiv:1511.07436] [INSPIRE].

[91] H.K. Dreiner, J.Y. Günther and Z.S. Wang, *R-parity violation and light neutralinos at ANUBIS and MAPP*, *Phys. Rev. D* **103** (2021) 075013 [arXiv:2008.07539] [INSPIRE].

[92] H.K. Dreiner, D. Köhler, S. Nangia and Z.S. Wang, *Searching for a single photon from lightest neutralino decays in R-parity-violating supersymmetry at FASER*, *JHEP* **02** (2023) 120 [arXiv:2207.05100] [INSPIRE].

[93] J.R. Ellis et al., *Astrophysical constraints on massive unstable neutral relic particles*, *Nucl. Phys. B* **373** (1992) 399 [INSPIRE].

[94] H.K. Dreiner and S. Grab, *All possible lightest supersymmetric particles in R-parity violating mSUGRA*, *Phys. Lett. B* **679** (2009) 45 [arXiv:0811.0200] [INSPIRE].

[95] D. Dercks et al., *R-parity violation at the LHC*, *Eur. Phys. J. C* **77** (2017) 856 [arXiv:1706.09418] [INSPIRE].

[96] H.K. Dreiner, F. Staub, A. Vicente and W. Porod, *General MSSM signatures at the LHC with and without R-parity*, *Phys. Rev. D* **86** (2012) 035021 [arXiv:1205.0557] [INSPIRE].

JHEP07(2023)215

[97] P. Konar, K.T. Matchev, M. Park and G.K. Sarangi, *How to look for supersymmetry under the lamppost at the LHC*, *Phys. Rev. Lett.* **105** (2010) 221801 [arXiv:1008.2483] [INSPIRE].

[98] CMS collaboration, *Search for new physics in events with two soft oppositely charged leptons and missing transverse momentum in proton-proton collisions at* $\sqrt{s} = 13$ *TeV*, *Phys. Lett. B* **782** (2018) 440 [arXiv:1801.01846] [INSPIRE].

[99] ATLAS collaboration, *Search for electroweak production of charginos and sleptons decaying into final states with two leptons and missing transverse momentum in* $\sqrt{s} = 13$ *TeV pp collisions using the ATLAS detector*, *Eur. Phys. J. C* **80** (2020) 123 [arXiv:1908.08215] [INSPIRE].

[100] CMS collaboration, *Search for top squarks in R-parity-violating supersymmetry using three or more leptons and B-tagged jets*, *Phys. Rev. Lett.* **111** (2013) 221801 [arXiv:1306.6643] [INSPIRE].

[101] CMS collaboration, *Search for physics beyond the Standard Model in multilepton final states in proton-proton collisions at* $\sqrt{s} = 13$ *TeV*, *JHEP* **03** (2020) 051 [arXiv:1911.04968] [INSPIRE].

[102] ATLAS collaboration, *Search for new phenomena in three- or four-lepton events in pp collisions at* $\sqrt{s} = 13$ *TeV with the ATLAS detector*, *Phys. Lett. B* **824** (2022) 136832 [arXiv:2107.00404] [INSPIRE].

[103] ATLAS collaboration, *Search for lepton-flavor violation in different-flavor, high-mass final states in pp collisions at* $\sqrt{s} = 13$ *TeV with the ATLAS detector*, *Phys. Rev. D* **98** (2018) 092008 [arXiv:1807.06573] [INSPIRE].

[104] ATLAS collaboration, *Search for type-III seesaw heavy leptons in leptonic final states in pp collisions at* $\sqrt{s} = 13$ *TeV with the ATLAS detector*, *Eur. Phys. J. C* **82** (2022) 988 [arXiv:2202.02039] [INSPIRE].

[105] ATLAS collaboration, *Search for heavy Higgs bosons decaying into two tau leptons with the ATLAS detector using pp collisions at* $\sqrt{s} = 13$ *TeV*, *Phys. Rev. Lett.* **125** (2020) 051801 [arXiv:2002.12223] [INSPIRE].

[106] CMS collaboration, *Searches for R-parity-violating supersymmetry in pp collisions at* $\sqrt{s} = 8$ *TeV in final states with* 0-4 *leptons*, *Phys. Rev. D* **94** (2016) 112009 [arXiv:1606.08076] [INSPIRE].

[107] ATLAS collaboration, *Search for supersymmetry in events with four or more charged leptons in* $139\,fb^{-1}$ *of* $\sqrt{s} = 13$ *TeV pp collisions with the ATLAS detector*, *JHEP* **07** (2021) 167 [arXiv:2103.11684] [INSPIRE].

[108] CMS collaboration, *Search for pair-produced resonances decaying to quark pairs in proton-proton collisions at* $\sqrt{s} = 13$ *TeV*, *Phys. Rev. D* **98** (2018) 112014 [arXiv:1808.03124] [INSPIRE].

[109] CMS collaboration, *Search for resonant and nonresonant production of pairs of dijet resonances in proton-proton collisions at* $\sqrt{s} = 13$ *TeV*, arXiv:2206.09997 [INSPIRE].

[110] ATLAS collaboration, *A search for pair-produced resonances in four-jet final states at* $\sqrt{s} = 13$ *TeV with the ATLAS detector*, *Eur. Phys. J. C* **78** (2018) 250 [arXiv:1710.07171] [INSPIRE].

[111] ATLAS collaboration, *Search for R-parity-violating supersymmetric particles in multi-jet final states produced in p-p collisions at* $\sqrt{s} = 13$ *TeV using the ATLAS detector at the LHC*, *Phys. Lett. B* **785** (2018) 136 [arXiv:1804.03568] [INSPIRE].

JHEP07(2023)215

[112] CMS collaboration, *Search for pair-produced three-jet resonances in proton-proton collisions at* $\sqrt{s} = 13$ *TeV*, *Phys. Rev. D* **99** (2019) 012010 [arXiv:1810.10092] [INSPIRE].

[113] ATLAS collaboration, *Search for phenomena beyond the Standard Model in events with large b-jet multiplicity using the ATLAS detector at the LHC*, *Eur. Phys. J. C* **81** (2021) 11 [*Erratum ibid.* **81** (2021) 249] [arXiv:2010.01015] [INSPIRE].

[114] CMS collaboration, *Search for pair-produced resonances each decaying into at least four quarks in proton-proton collisions at* $\sqrt{s} = 13$ *TeV*, *Phys. Rev. Lett.* **121** (2018) 141802 [arXiv:1806.01058] [INSPIRE].

[115] CMS collaboration, *Search for new phenomena in events with high jet multiplicity and low missing transverse momentum in proton-proton collisions at* $\sqrt{s} = 8$ *TeV*, *Phys. Lett. B* **770** (2017) 257 [arXiv:1608.01224] [INSPIRE].

[116] CMS collaboration, *Search for R-parity violating supersymmetry in pp collisions at* $\sqrt{s} = 13$ *TeV using b jets in a final state with a single lepton, many jets, and high sum of large-radius jet masses*, *Phys. Lett. B* **783** (2018) 114 [arXiv:1712.08920] [INSPIRE].

[117] CMS collaboration, *Search for pair-produced vector-like leptons in final states with third-generation leptons and at least three b quark jets in proton-proton collisions at* $\sqrt{s} = 13$ *TeV*, arXiv:2208.09700 [INSPIRE].

[118] CMS collaboration, *Search for R-parity violating decays of a top squark in proton-proton collisions at* $\sqrt{s} = 8$ *TeV*, *Phys. Lett. B* **760** (2016) 178 [arXiv:1602.04334] [INSPIRE].

[119] ATLAS collaboration, *Search for direct production of electroweakinos in final states with one lepton, jets and missing transverse momentum and in pp collisions at* $\sqrt{s} = 13$ *TeV with the ATLAS detector*, ATLAS-CONF-2022-059, CERN, Geneva, Switzerland (2022).

[120] CMS collaboration, *Search for singly and pair-produced leptoquarks coupling to third-generation fermions in proton-proton collisions at* $\sqrt{s} = 13$ *TeV*, *Phys. Lett. B* **819** (2021) 136446 [arXiv:2012.04178] [INSPIRE].

[121] ATLAS collaboration, *Search for direct production of winos and higgsinos in events with two same-sign or three leptons in pp collision data at* $\sqrt{s} = 13$ *TeV with the ATLAS detector*, ATLAS-CONF-2022-057, CERN, Geneva, Switzerland (2022).

[122] ATLAS collaboration, *Search for B-L R-parity-violating top squarks in* $\sqrt{s} = 13$ *TeV pp collisions with the ATLAS experiment*, *Phys. Rev. D* **97** (2018) 032003 [arXiv:1710.05544] [INSPIRE].

[123] ATLAS collaboration, *Search for pair-produced scalar and vector leptoquarks decaying into third-generation quarks and first- or second-generation leptons in pp collisions with the ATLAS detector*, *JHEP* **2306** (2023) 188 [arXiv:2210.04517] [INSPIRE].

[124] ATLAS collaboration, *Search for pair production of scalar leptoquarks decaying into first- or second-generation leptons and top quarks in proton-proton collisions at* $\sqrt{s} = 13$ *TeV with the ATLAS detector*, *Eur. Phys. J. C* **81** (2021) 313 [arXiv:2010.02098] [INSPIRE].

[125] CMS collaboration, *Search for an excited lepton that decays via a contact interaction to a lepton and two jets in proton-proton collisions at* $\sqrt{s} = 13$ *TeV*, *JHEP* **05** (2020) 052 [arXiv:2001.04521] [INSPIRE].

[126] ATLAS collaboration, *Search for pair production of squarks or gluinos decaying via sleptons or weak bosons in final states with two same-sign or three leptons with the ATLAS detector*, ATLAS-CONF-2023-017, CERN, Geneva, Switzerland (2023).

JHEP07(2023)215

[127] ATLAS collaboration, *Search for pair production of higgsinos in final states with at least three b-tagged jets in $\sqrt{s} = 13$ TeV pp collisions using the ATLAS detector*, *Phys. Rev. D* **98** (2018) 092002 [arXiv:1806.04030] [INSPIRE].

[128] CMS collaboration, *Search for Higgsino pair production in pp collisions at $\sqrt{s} = 13$ TeV in final states with large missing transverse momentum and two Higgs bosons decaying via $H \to b\bar{b}$*, *Phys. Rev. D* **97** (2018) 032007 [arXiv:1709.04896] [INSPIRE].

[129] J. Alwall et al., *The automated computation of tree-level and next-to-leading order differential cross sections, and their matching to parton shower simulations*, *JHEP* **07** (2014) 079 [arXiv:1405.0301] [INSPIRE].

[130] T. Sjöstrand et al., *An introduction to PYTHIA* 8.2, *Comput. Phys. Commun.* **191** (2015) 159 [arXiv:1410.3012] [INSPIRE].

[131] B. Fuks, *The Minimal Supersymmetric Standard Model with R-parity violation*, https://feynrules.irmp.ucl.ac.be/wiki/RPVMSSM, accessed 1 December 2021.

[132] D. Dercks et al., *CheckMATE* 2*: from the model to the limit*, *Comput. Phys. Commun.* **221** (2017) 383 [arXiv:1611.09856] [INSPIRE].

[133] M. Cacciari, G.P. Salam and G. Soyez, *FastJet user manual*, *Eur. Phys. J. C* **72** (2012) 1896 [arXiv:1111.6097] [INSPIRE].

[134] M. Cacciari and G.P. Salam, *Dispelling the N^3 myth for the k_t jet-finder*, *Phys. Lett. B* **641** (2006) 57 [hep-ph/0512210] [INSPIRE].

[135] M. Cacciari, G.P. Salam and G. Soyez, *The anti-k_t jet clustering algorithm*, *JHEP* **04** (2008) 063 [arXiv:0802.1189] [INSPIRE].

[136] A.L. Read, *Presentation of search results: the CL_s technique*, *J. Phys. G* **28** (2002) 2693 [INSPIRE].

[137] *CheckMATE (Check Models At Terascale Energies) webpage*, https://checkmate.hepforge.org/, accessed 1 December 2022.

[138] DELPHES 3 collaboration, *DELPHES* 3*, a modular framework for fast simulation of a generic collider experiment*, *JHEP* **02** (2014) 057 [arXiv:1307.6346] [INSPIRE].

[139] ATLAS collaboration, *Search for supersymmetry in final states with two same-sign or three leptons and jets using 36 fb^{-1} of $\sqrt{s} = 13$ TeV pp collision data with the ATLAS detector*, *JHEP* **09** (2017) 084 [*Erratum ibid.* **08** (2019) 121] [arXiv:1706.03731] [INSPIRE].

[140] C. Borschensky et al., *Squark and gluino production cross sections in pp collisions at $\sqrt{s} = 13$, 14, 33 and 100 TeV*, *Eur. Phys. J. C* **74** (2014) 3174 [arXiv:1407.5066] [INSPIRE].

[141] S. Bornhauser, M. Drees, H.K. Dreiner and J.S. Kim, *Electroweak contributions to squark pair production at the LHC*, *Phys. Rev. D* **76** (2007) 095020 [arXiv:0709.2544] [INSPIRE].

JHEP07(2023)215